Aerosol Science and Technology, 46:1201–1218, 2012
Copyright © American Association for Aerosol Research
ISSN: 0278-6826 print / 1521-7388 online
DOI: 10.1080/02786826.2012.701784

Downloaded by [Institute Of Atmospheric Physics] at 20:09 13 July 2012

Pollution Gradients and Chemical Characterization of Particulate Matter from Vehicular Traffic near Major Roadways: Results from the 2009 Queens College Air Quality Study in NYC

Paola Massoli,[1] Edward C. Fortner,[1] Manjula R. Canagaratna,[1] Leah R. Williams,[1] Qi Zhang,[2] Yele Sun,[3] James J. Schwab,[4] Achim Trimborn,[5] Timothy B. Onasch,[1] Kenneth L. Demerjian,[4] Charles E. Kolb,[1] Douglas R. Worsnop,[1] and John T. Jayne[1]

[1]*Aerodyne Research Inc., Billerica, Massachusetts, USA*
[2]*Department of Environmental Toxicology, University of California, Davis, California, USA*
[3]*Department of Chemistry, State Key Laboratory of Atmospheric Boundary Layer Physics and Atmospheric, Institute of Atmospheric Physics, Chinese Academy of Sciences, Beijing, China*
[4]*Atmospheric Sciences Research Center, State University of New York at Albany, Albany, New York, USA*
[5]*AeroMegt GmBH., Hilden, Germany*

We present measurements of traffic-related pollutants made near the Long Island Expressway (LIE, I-495), in Queens, New York. The Aerodyne Research Inc. (ARI) mobile laboratory (AML) was deployed to map spatial and temporal gradients of gas-phase species and particulate matter (PM) associated with vehicular exhaust in the residential areas near the LIE. We observe that pollutant levels build up during the early morning hours under stable boundary layer conditions yet fall off quickly within 150 m downwind of the highway. An ARI soot particle aerosol mass spectrometer (SP-AMS) provided measurements of the size-resolved chemical composition of refractory black carbon (rBC) and the associated coating species. The average size distribution of the traffic related PM is characterized by a rBC mode centered at ∼100 nm in vacuum aerodynamic diameter, D_{va} (rBC mass fraction ∼50%). A second rBC mode (rBC mass fraction ∼5%) more heavily coated with organic material is also observed at D_{va} ∼500 nm. Positive matrix factorization (PMF) analyses of the traffic-related PM indicates that rBC is mostly associated with hydrocarbon-like organic (HOA) PM. These results are discussed in the context of chemically resolved size distributions and PMF analysis results performed on the SP-AMS stationary data collected at the Queens College site. Finally, we report emission indices (EI) for both fleet-average conditions and single vehicles, including several New York City Metropolitan Transit Authority (MTA) buses, sampled by the AML in "chase" mode during the study.

[Supplementary materials are available for this article. Go to the publisher's online edition of *Aerosol Science and Technology* to view the free supplementary files.]

1. INTRODUCTION

On-road motor vehicles are the largest source of gas-phase and particulate matter (PM) pollutants in both urban environments (WHO 2002) and moderately industrialized areas (Zou et al. 2009). Traffic-related combustion products (CO_2 and black carbon, BC) exert a warming effect on the Earth's radiative balance (Jacobson et al. 2001; IPCC 2007), and they are directly responsible for air quality and visibility degradation (Watson 2002). Epidemiological and toxicological studies show that both acute and chronic exposure to traffic emissions pose serious health threats, as combustion exhaust products have been linked to pulmonary and cardiovascular diseases as well as to neurodegenerative, carcinogenic, and mutagenetic effects (Brunekreef et al. 1997; Pope et al. 2002; Pedersen et al. 2004; Pope and Dockery 2006; Brugge et al. 2007; Dockery and Stone 2007; Green et al. 2009; Russell and Brunekreef 2009; Di Filippo et al. 2010; Stanek et al. 2011). Recent work indicates that life expectancy can significantly improve upon reduction in

Received 19 January 2012; accepted 16 May 2012.
Paola Massoli thanks Dr. Andrew Freedman for supporting the deployment of the CAPS PMex monitor during the QC study, and Dr. Ezra Wood and Dr. Scott Herndon for useful discussion. The authors thank the New York State Department of Environmental Conservation for use of their facility, and the Queens College administration and staff. This study was partially supported by Department of Energy (DoE) project # DE-F602–07ER.
Address correspondence to Paola Massoli, Aerodyne Research Inc., 45 Manning Road, Billerica, MA, 02145, USA. E-mail: pmassoli@aerodyne.com

Downloaded by [Institute Of Atmospheric Physics] at 20:09 13 July 2012

personal exposure to urban ambient air pollution (Pope et al. 2009).

Both the quantification and the chemical characterization of traffic related emissions (as well as of other forms of transportation and residential combustion products) have gained increasing attention in the last few years. Several measures have been implemented by the U.S. Environmental Protection Agency (EPA) in order to regulate traffic related emissions of harmful gas phase species and total PM mass in the supermicron and submicron size ranges (EPA 2008). Increasing attention has also been dedicated toward measuring the number of traffic-related particles in the ultrafine size range (mobility diameter $<$100 nm), especially near major roadways. Although ultrafine particulate matter (UFPM) may contribute a minor fraction of total mass from vehicle emissions (Zhu et al. 2002a), UFPM is potentially harmful because of its toxicity (Dockery et al. 1993; Knol et al. 2009) and capability to deposit deeply in lungs (Morawska et al. 2008; Lubick 2009). Seigneur (2009) gives a comprehensive summary of the current understanding and the challenges associated with measuring and characterizing UFPM emitted from mobile sources. Supermicron PM associated with traffic, such as re-suspended dust and tire abrasion products, is also of concern (Gehrig et al. 2004; Bukowiecki et al. 2010; Kupianen and Pirjola 2011), and the specific health effects of size-segregated traffic related PM have been investigated (Perez et al. 2009).

The characterization of vehicular PM both near and downwind of major sources is challenging because of the rapid changes in particle number concentration, composition, and size distribution that vehicle exhaust undergoes after emission due to dilution and atmospheric processing (Canagaratna et al. 2010). Dispersion and evolution of near-roadway pollutants is highly dependent on traffic patterns, meteorology (wind speed, wind direction, and temperature) as well as atmospheric stability, for example, boundary layer height (Zhu et al. 2006; Beckerman et al. 2008; Hagler et al. 2009; Hu et al. 2009). To date, several studies have reported highly resolved descriptions of spatial and temporal dispersion patterns of roadside pollutants (Zhu et al. 2002a,b, 2004; Zhang et al. 2004, 2005a; Pirjola et al. 2006; McAuley 2010). Such information is critical to properly quantifying the health effects of personal exposure to near-roadways pollution. Durant et al. (2010) deployed the Aerodyne Research Inc. (ARI) mobile laboratory (AML) to characterize pollution gradients near a major highway in Somerville, Massachusetts, during the weekday morning traffic peak. Consistently with previous literature (Karner et al. 2010, and references therein), one of the main findings of the study was that traffic-related pollutants decrease sharply with distance from road sources.

During the summer 2009, Field Intensive Study at Queens College (QC), New York, the AML was deployed from 13 July to 1 August on the QC campus with the goal of characterizing the area's air quality. This 2009 study represented the third major field study at QC following the deployments of summer 2001 and winter 2004 (Canagaratna et al. 2004; Drewnick et al. 2004a,b; Dutkiewicz et al. 2004, 2006; Shorter et al. 2005; Weimer et al. 2006; Demerjian and Mohnen 2008). The QC site was located ~450 m south of the Long Island Expressway (LIE, I-495), a major highway running for 70 miles across Long Island. The AML was equipped with instrumentation to measure selected gas phase species (CO_2, NO, and NO_2) as well as particle microphysical properties (number concentration and size distribution) and chemical composition. Aerosol optical properties (light extinction and light absorption) were also measured to estimate the single scattering albedo (ω) of aerosol particles. The SUNY Albany mobile facility ASRC-ML (Lin et al. 2011) was also deployed at the QC site during the same time to perform real-time gas phase and particle measurements. Sun et al. (2011a,b, 2012) present a comprehensive characterization of the nonrefractory PM_1 measured by an ARI high resolution aerosol time of flight mass spectrometer (HR-AMS) deployed on the ASRC-ML, and show that secondary organic aerosols (SOA) dominated the PM_1 concentrations at the QC site. A similar result is reported by Ng et al. (2011a) based on the data from an ARI Aerosol Chemical Speciation Monitor (ACSM) deployed 100 m north of the QC site.

This article mainly focuses on a specific subset of the 2009 QC campaign dataset, consisting of mobile measurements performed with the ARI AML near the LIE. Measurements were made during the morning rush hours (from 04:30 to 09:30 AM) both upwind and downwind of the LIE to characterize the spatial and temporal evolution of pollutants in the residential neighborhoods. The chemical composition of the traffic-related PM was measured using an ARI soot particle time of flight (pToF) aerosol mass spectrometer, SP-AMS (Onasch et al. 2012). The SP-AMS provided new insights on the size-resolved chemical composition of the refractory BC (rBC) and associated coating species directly related to traffic emissions. In addition to the measurements performed directly downwind of the LIE, we discuss key features of the SP-AMS stationary data collected at the QC site, and compare those results with data obtained by the co-located HR-AMS (Sun et al. 2011a). Chemical signature and particle sizing for single motor vehicle exhaust plumes sampled during "chase studies," including several buses operated by the New York City Metropolitan Transit Authority (MTA) are also presented. Vehicle-specific pollutant footprints (emission indices, [EI]) are reported for both on-road average traffic conditions and individually chased vehicles.

2. EXPERIMENTAL METHODS

2.1. AML Measurements

The AML (Kolb et al. 2004) is a modified 1989 Ford gasoline powered vehicle carrying state-of-the-art instrumentation for real-time monitoring of both gas-phase and particulate species. The AML has been deployed in a wide range of field experiments measuring, for example, emissions from motor vehicles and aircrafts engines (Canagaratna et al. 2004; Herndon et al.

Downloaded by [Institute Of Atmospheric Physics] at 20:09 13 July 2012

2005; Onasch et al. 2009; Durant et al. 2010). During the QC study, the AML was equipped with a commercial CO_2 analyzer (Model 820, Li-COR); a chemi-luminescence analyzer for NO_2, NO, and total NO_x (NO plus NO_2) measurements (Model 42i, Thermo Environmental); an ultraviolet O_3 monitor (Model 205, 2B-Tech); a butanol-based Condensation Particle Counter (CPC, Model 3022A TSI) for submicron total particle number concentration; a scanning mobility particle sizer (SMPS, TSI) for size distribution measurements in the submicron range, comprising a model 3080 electrostatic classifier (DMA) and a model 3776 CPC; a cavity attenuated phase shift particle extinction monitor (CAPS PMex, ARI) to measure PM light extinction at 630 nm (Massoli et al. 2010); a multiangle absorption photometer (MAAP, Thermo Environmental) to measure PM light absorption also at 630 nm (Petzold et al. 2005 and references therein); and a ARI SP-AMS for the chemical composition of refractory PM (Onasch et al. 2012). Combination of the CAPS PMex extinction and MAAP absorption yielded the PM single scattering albedo (ω) at 630 nm.

The AML has two separate inlets: the gas phase species are sampled through teflon tubing (equipped with a 0.45 μm teflon filter for removing particles) whereas the particles are sampled through a second inlet made of copper tubing and equipped with a $PM_{2.5}$ cyclone impactor (URG-2000–30EN). All aerosol instruments were downstream of the same $PM_{2.5}$ inlet. However, the detected size range of the SMPS and the SP-AMS are smaller than that transmitted by the cyclone. The SMPS scans were performed between 15 and 690 nm, and the SP-AMS reported the composition of PM_1 based on the transmission characteristics of the standard aerodynamic lens which has a 50% cut-off below 80 nm and above 600 nm in vacuum aerodynamic diameter, D_{va} (Liu et al. 2007).

Calibrations of both CO_2 and NO_x analyzers were performed routinely following the same methods described in Durant et al. (2010). Filtered air was collected through the PM inlet for routine zeroing of the PM measurements; in addition, the CAPS PMex was set to self-calibrate by an automated zeroing procedure as described in Massoli et al. (2010). The MAAP data were analyzed following the method described in Petzold and Schönlinner (2004) and a MAAP-based BC concentration was obtained from the 630 nm light absorption using a mass specific absorption cross section of 6.6 $m^2\ g^{-1}$ (Petzold et al. 2002). All instruments were operated at 1 s time resolution, except for the SP-AMS (15 s) and the SMPS (120 s).

2.2. Gradient Measurements: Characteristics of the Study Area and Sampling Strategy

According to the New York State Department of Transportation (NYSDOT), the LIE handles approximately 210,000 vehicles per day through Queens. Because the LIE is a route for commuter and commercial traffic, it is transited by both heavy duty (HD) and low-duty (LD) vehicles. In Queensborough, the LIE has three east-bound and three west-bound lanes, and a two-lane frontage road (the Horace Harding Expressway [HHE]) on each side. Figure 1 shows the area chosen to perform the pollution gradient experiments, which included the residential blocks situated between the QC site (500 m south of LIE, parking lot#6) and Booth Memorial Drive (500 m north of the LIE) in the N–S direction, and between Kissena Boulevard and Main Street in the E–W direction ($\sim$600 m in horizontal distance). The residential buildings in this neighborhood are located on both sides of the LIE and are identical three-story high complexes with flat roofs. The street blocks are about 100 m wide, and the first inhabited block is situated along the HHE ($\sim$10 m from the LIE). The area does not have other major traffic emission sources, as the closest highway, I-678, is located 1.2 km to the east.

Early morning hours ($\sim$04:30–09:30 Eastern Daylight Time [EDT]) were chosen because morning emissions are confined in the shallow boundary layer, and pollution gradients can be easily mapped. The meteorology of the area during the 3-week-long campaign was characterized by South-South West (SW) winds with speeds generally lower than 4 m s^{-1} (Sun et al. 2011a). Under these conditions, the north and south sides of the LIE are respectively downwind and upwind of traffic emissions. The AML was driven alternatively on the downwind and upwind sides of the LIE following a raster-driving pattern at steady driving speed of 10 m s^{-1}. Five loops in the downwind side ($\sim$40 min each) and three loops in the upwind side ($\sim$20 min each) could be completed during a 5-h experiment. Vehicular traffic was very light on the neighborhoods' streets until 07:30, allowing the AML to maintain constant driving speed and to avoid data contamination due to traffic emissions not related to the LIE. Because traffic was generally heavier on the boundary roads, the time periods corresponding to transit along Main Street and Kissena Blvd were removed from the dataset. Additional self-sampling artifacts and other emissions not associated with traffic from the LIE were removed using wind data recorded by the anemometer located near the particle inlet.

This sampling protocol was performed on two mornings (28 July and 31 July) characterized by stagnant conditions with light ($<$2 m s^{-1}) and stable S–SW winds. Here, we mainly discuss the results from 28 July and report merged results from both days only when possible, since the sampling on 31 July was interrupted around 06:30 by heavy rain. On the morning of July 28, the ASRC-ML was also deployed to measure roadside traffic emissions and it stationed approximately 30 m upwind of the LIE between 04:40 and 09:30 (Sun et al. 2012). The data in this study are reported in local time (i.e., EDT), which equals Coordinated Universal Time (UTC) minus 5 h.

2.3. Soot Particle Aerosol Mass Spectrometer (SP-AMS)

The SP-AMS is a novel ARI development that combines two state-of-the-art instruments: (1) the Droplet Measurements Technologies (DMT) Single Particle Soot Photometer (SP2) for measurements of refractory black carbon (rBC) (Schwarz et al. 2006) and (2) the ARI HR-AMS (DeCarlo et al. 2006) for the chemical analysis of bulk nonrefractory PM_1 (NR-PM_1). The SP-AMS features a SP2 1064 nm continuous wave (CW)

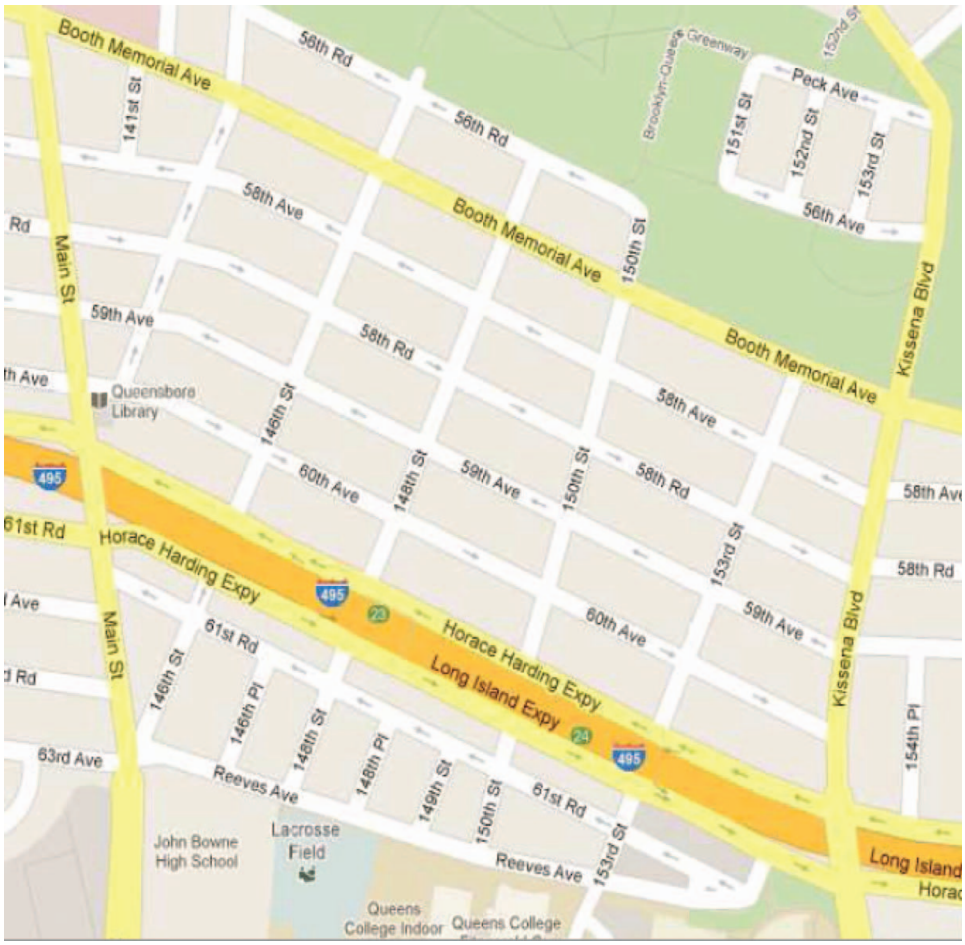

FIG. 1. Map of the study area for the mobile measurements of 28 July (0430–0845, EDT) and 31 July (0430–0630, EDT) 2009. On both days, winds were light (<2 m s^{-1}) and coming from S-SW. AML was driven alternatively on the upwind (south) and downwind (north) of the LIE following a raster driving pattern. The QC site is located 450 m south of the LIE.

intra cavity laser inserted into a HR-AMS chamber perpendicularly to the particle beam axis. The laser allows to vaporize rBC-containing particles under SP2-like incandescence conditions (Gao et al. 2007) rather than at the standard AMS's tungsten vaporizer temperature of 600°C. In the SP-AMS, particles are first aerodynamically focused into the laser beam. As rBC-containing particles are heated by laser absorption, the PM associated with rBC (coating material) is vaporized, generating neutral chemical species. The removal of the coating allows the rBC core to heat up further, incandesce and vaporize into neutral carbon clusters. The resulting molecular vapor is ionized via 70 eV electron impact, and subsequent ion detection and chemical characterization occur via standard HR-AMS spectrometry (Canagaratna et al. 2007). The higher particle temperature attained by laser heating compared to the tungsten vaporizer extends the range of detectable coating material associated with rBC. Here, we use the term coating PM (hereafter cPM) to indicate the total coating material measured by the SP-AMS, which may include components that by definition are both non-refractory and refractory, that is, that vaporize in the laser below and above 600°C, respectively. Instrument calibration with regal black particles (Regal 400R pigment, Cabot Corp.) is applied for rBC quantification, yielding a specific rBC ionization efficiency (mIE_{rBC}), or instrument sensitivity, greater than 140 ± 6 carbon ions detected per picogram of rBC mass sampled (ions/pg). The 3-σ detection limit for rBC is <0.1 μg m^{-3} for 60 s averaging. The mIE_{rBC} depends on both laser-particle beam overlap and ion optics tuning of the instrument. The experimentally determined mass-specific ionization efficiency of rBC relative to particulate nitrate (rBC relative ionization efficiency, RIE_{rBC}) is 0.2 ± 0.1 (2-σ uncertainty). The SP-AMS calibration and rBC quantification methods, as well as instrument operating principles and modalities, are discussed extensively in Onasch et al. (2012).

For the measurements reported here, the SP-AMS was operated in the laser-only configuration (i.e., the tungsten vaporizer was removed) and in the more sensitive *V* ion time of flight mode. Note that in the laser-only configuration, the SP-AMS detects exclusively particles that absorb at 1064 nm, that is,

Downloaded by [Institute Of Atmospheric Physics] at 20:09 13 July 2012

Downloaded by [Institute Of Atmospheric Physics] at 20:09 13 July 2012

rBC-containing particles and their associated coating (cPM). Data acquisition alternated between mass spectrum (MS) and pToF modes, with a time resolution of 15 s. The SP-AMS data were analyzed using the high resolution AMS data analysis software packages PIKA v.1.10H and APES v.1.05A (Sueper 2010). Positive matrix factorization (PMF) analyses were also performed using the PMF2.exe algorithm (v.4.2) in robust mode (Paatero and Tapper 1994). The PMF inputs (mass spectral and error matrices) were prepared according to Zhang et al. (2011). The PMF2 solutions were then evaluated with an Igor Pro-based PMF Evaluation Tool (PET, v. 2.04), following the method described in Ulbrich et al. (2009) and Zhang et al. (2011).

2.4. EI Calculations

On-road vehicles are characterized by a wide range of sizes, combustion efficiency, exhaust treatment, etc., resulting in highly diversified emission footprints (emissions index, EI). For example, HD vehicles are typically powered by diesel engines and emit more BC per unit of fuel burnt compared to LD gasoline-powered vehicles (Imhof et al. 2006; Ban-Weiss et al. 2007; Strawa et al. 2010). In addition, Kleeman et al. (2000) and Schauer et al. (2002) report relative larger organic carbon (OC) emissions and lower elemental carbon (EC) from LD vehicles compared to HD vehicles. EIs are required to compile inventories and define standards to properly regulate harmful emissions (Maricq and Maldonado 2009). EI values reported in this work are calculated as the enhancement of the pollutant X above background with respect to CO_2 following the method of Canagaratna et al. (2004) and Herndon et al. (2005), and described in Equation (1)

$$\mathrm{EI} = \Delta X/\Delta \mathrm{CO_2} * f_{\mathrm{fuel}} \quad [1]$$

where $\Delta X/\Delta CO_2$ is the increment above background for the X species and CO_2, and f_{fuel} is a multiplicative factor that includes (1) w_c, the weight fraction of carbon in the fuel and (2) the conversion of CO_2 in units of ppm to units of μg of carbon per m^{-3}. A 100% combustion efficiency in the conversion of fuel to CO_2 is assumed. Typical values for w_c are 0.85 for gasoline and 0.87 for diesel fuel (Kirchstetter et al., 1999). In this study, we used an average $w_c = 0.86$, which yields a $f_{\mathrm{fuel}} = 1.762$ for ambient T (290 K) and P (760 torr). The EI values are expressed in units of g of pollutant per kg of fuel burned (g kg^{-1}) for mass-based measurements, and in m^2 kg^{-1} for optical quantities as in Ban-Weiss et al. (2007). During the QC campaign, measurements of CO and hydrocarbon (HC) species, also emitted by vehicle exhaust, were not available. However, the systematic error in EI estimates that arises from not including CO is small, that is, between 0.7 and 3% for EI_{CO} ranging from 15 to 60 g kg^{-1}, a value typically observed in traffic related emissions (Ban-Weiss et al. 2008; Durant et al. 2010).

3. RESULTS AND DISCUSSION

3.1. Spatial-Temporal Gradients of Traffic-Related Gas Phase and Particle Species

Figures 2 and 3 show an overview of the spatial and temporal concentration gradients measured upwind and downwind of the LIE (left and right columns, respectively). The CO_2 (ppmv), NO (ppbv), and NO_2 (ppbv) gradients are shown in Figure 2, whereas the particle number from CPC (p cm^{-3}), BC from MAAP (μg m^{-3}), and ω are shown in Figure 3. Each point is the average concentration measured at every street block. Data from both 28 July (04:30–08:45, EDT) and 31 July (04:30–06:30, EDT) are combined.

On the downwind side of the LIE, the concentrations for all the measured species (except NO_2, Figure 2c) are maximum for location closest to the highway and fall off as a function of distance, as expected mainly due to dilution effects (Zhang and Wexler 2004). The steepest drop occurs between 10 and 200 m downwind, with CO_2 (Figure 2a) and NO (Figure 2b) decreasing of 15–20%, and particle number (Figure 3a) and BC (Figure 3b) decreasing of ~60%. The ω gradients (Figure 3c) reflect the trends in BC, with ω values as low as 0.5 next to the LIE where the BC concentration is the highest, and up to 0.7 away as BC is progressively diluted with distance. The temporal trends indicate that pollution levels increase during the early morning hours and stay confined in the boundary layer. Concentrations are higher after 06:00, in synch with the observed traffic volume increase (Sun et al. 2012). The highest pollutant concentrations (and the lowest ω values) are observed between 06:15 and 07:30 across the downwind neighborhood. After 08:00, pollution levels stay elevated near the roadway, but they return to background values for locations greater than 200 m downwind of the LIE. This behavior is ascribed to the increase in the boundary layer depth after sunrise, which causes dispersion of ground-level pollutants (with sunrise, thermal heating of the surface induces mixing and entrainment of aged air from aloft, which typically is low in primary pollutants such as NO_x and higher in secondary pollutants, for example, O_3). Figure S1 (see supplemental information) shows such effect of boundary layer growth on the diurnal trends of NO_x and O_3 measured at the QC site between 13 July–3 August 2009. In the upwind neighborhood (left columns of Figures 2 and 3), the pollution levels are lower and the spatial-temporal trends are weaker, also in agreement with previous similar roadside mobile measurements (Durant et al. 2010).

As noted earlier, NO_2 (Figure 2c) does not exhibit any spatial trend; however, a NO_2 increase is observed after 0800 on both sides of the LIE. This suggests that most NO_2 is produced via oxidation of primary NO emissions after sunrise, when mixing of air from aloft increases the O_3 available for the conversion of NO to NO_2. Since NO_x emissions consist mainly of NO in the USA (Ban-Weiss et al. 2008), NO_2 concentrations near sources are mostly limited by the extent to which primary NO emissions can be converted to NO_2 by reaction with O_3 (Wood

Downloaded by [Institute Of Atmospheric Physics] at 20:09 13 July 2012

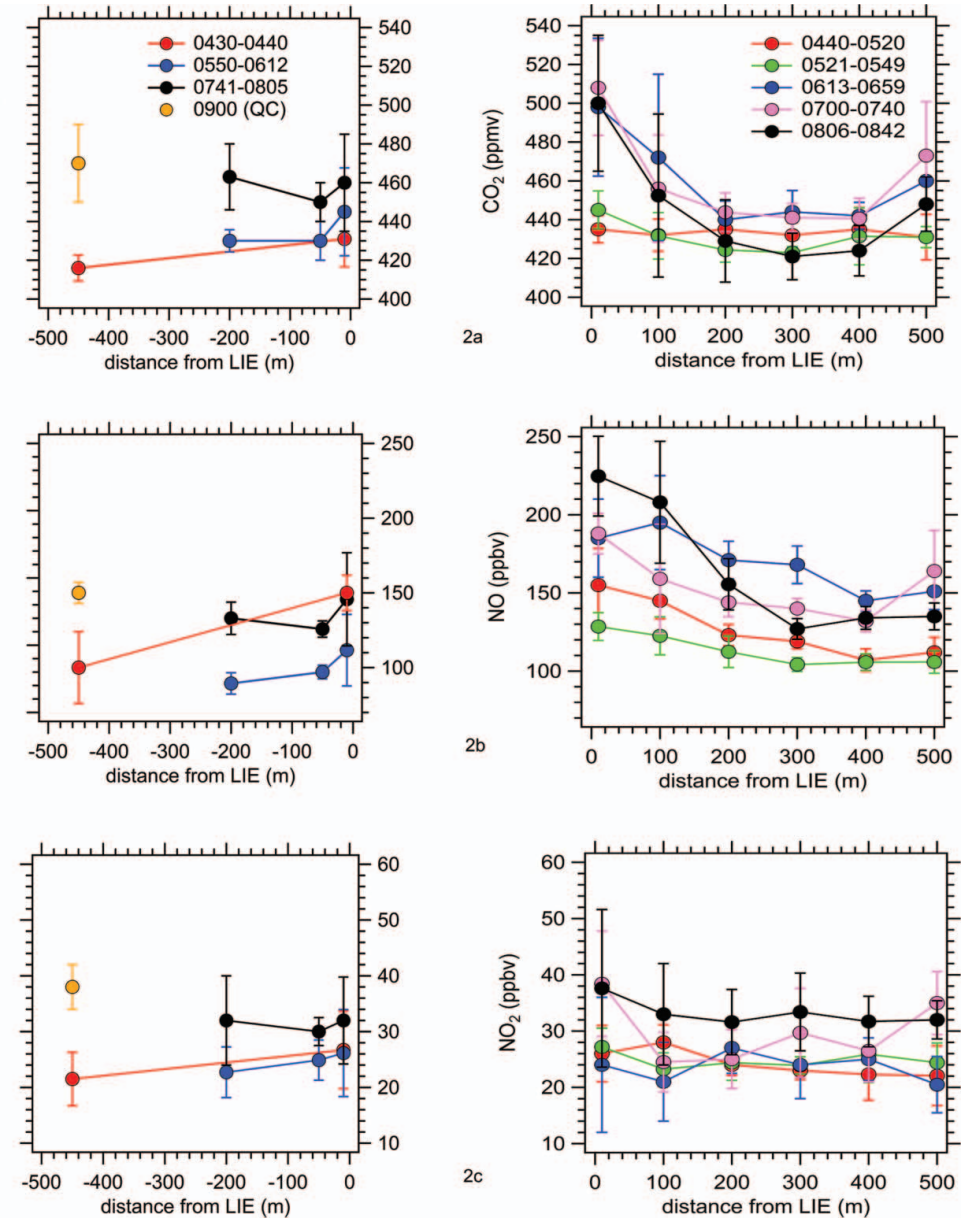

FIG. 2. Spatial and temporal concentration gradients of (a) CO_2, (b) NO, and (c) NO_2 measured both downwind and upwind of the LIE (right and left column, respectively). Lower pollution levels and no systematic trends characterize the upwind side of the highway. NO_2 shows a flat spatial trend, but increases after 0800 EDT. The error bars are the 1-σ standard deviation of data collected on both 28 and 31 July 2009.

et al., in prep.). For the near-road conditions presented here, NO_x values were above 100 ppbv and O_3 levels were as low as 5 ppbv (not shown). Since typical background levels of O_3 range from 20–45 ppbv (Chan et al. 2009), the low O_3 and NO_2 concentrations measured directly downwind of the LIE indicate that NO_2 had reached a "ceiling" value determined by the background O_3 levels. These NO_2 and O_3 trends are qualitatively consistent with the findings of Durant et al. (2010). Therefore, under the conditions examined here (short temporal scale and for distances $\leq$500 m for source), NO_2 alone is not a good "indicator" of traffic-related emissions.

The spatial and temporal trends of the SP-AMS-based rBC, cPM (in μg m^{-3}) and the rBC coating mass to rBC mass ratio (cPM/rBC) are shown in Figure S2. Only gradients downwind of the LIE are shown. As already pointed out, the cPM represents only the coating material associated with rBC cores. The trends of rBC and cPM are qualitatively consistent with the ones observed for the other traffic-related species (Figures 2 and 3). The slightly lower cPM/rBC values measured for locations $\leq$200 m downwind the LIE indicates the presence of less coated particles near source compared to, for example, 400 m away, suggesting that freshly emitted rBC particles have less coating mass than

Downloaded by [Institute Of Atmospheric Physics] at 20:09 13 July 2012

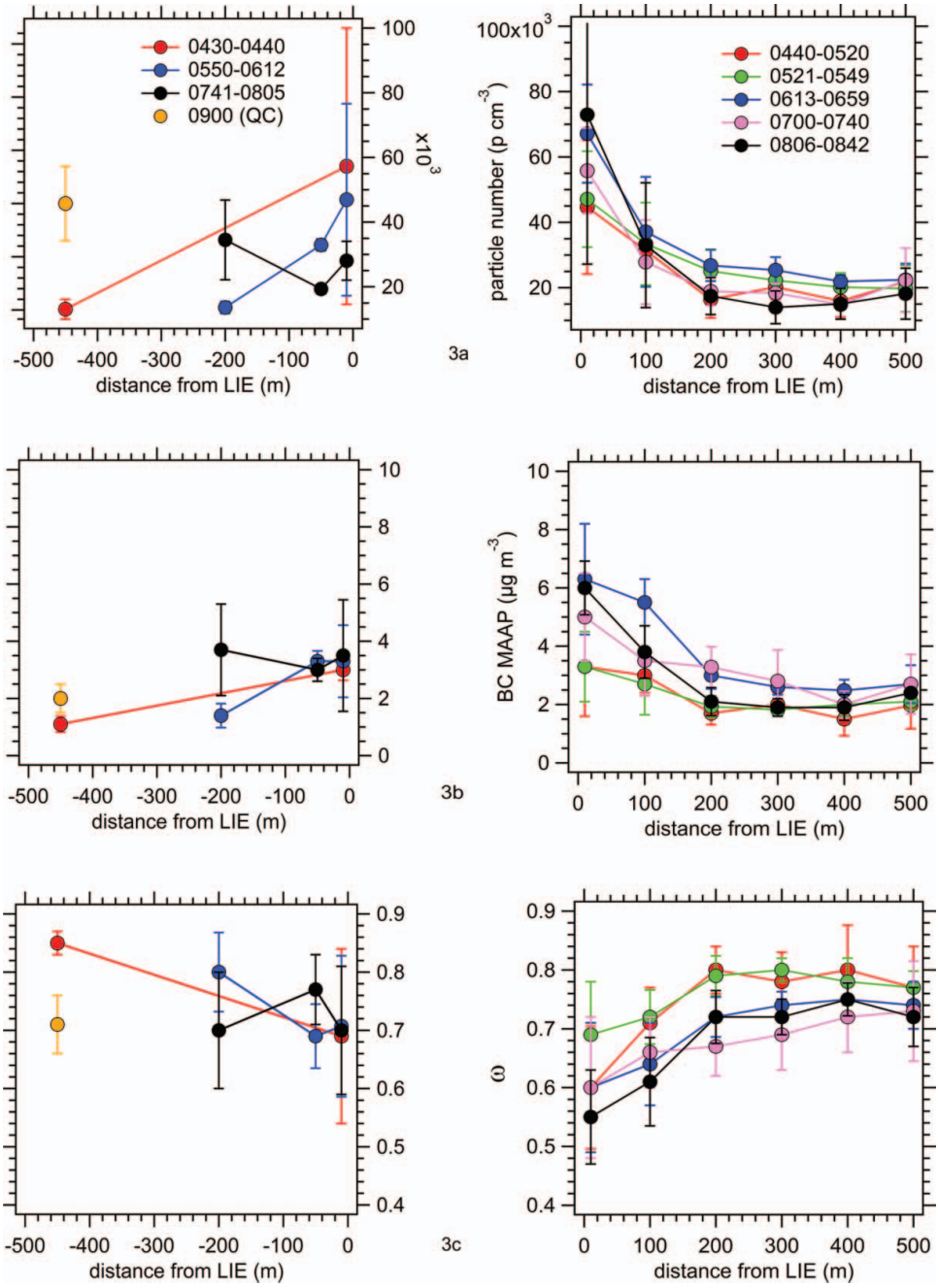

FIG. 3. Spatial and temporal concentration gradients of (a) particle number, (b) BC, and (c) ω reported for both the downwind and upwind side of the LIE (right and left column, respectively). The ω values are as low as 0.5 near the LIE. The trends of particle number and BC are qualitatively similar to those observed for CO_2 and NO, indicating that the LIE is the common source of these pollutants in the neighborhood. The error bars are the $1-\sigma$ standard deviation of data collected on both 28 July and 31 July 2009.

the "background" aerosol. We also notice that the cPM/rBC values initially decrease and then increase in time, with the lowest cPM/rBC values measured between 06:00 and 07:30 EDT at any given distance from the LIE. This trend suggests that the sampling before 06:00 may be dominated by background PM (more aged and more heavily coated rBC-containing particles) whereas freshly emitted and less coated particles dominate after 06:00, that is, when the increase in traffic volume observed on the LIE starts reflecting into the PM properties of the entire downwind neighborhood.

Downloaded by [Institute Of Atmospheric Physics] at 20:09 13 July 2012

3.2. PMF Analyses of the SP-AMS Gradient Measurements

In this section, we discuss PMF analyses for the SP-AMS gradient data collected on 28 July (04:30–08:45 EDT, that is, for both downwind and upwind transits). PMF was performed on the combined mass spectral matrices of ORG and rBC. The possibility of performing PMF on the combined ORG and rBC data allowed to extract quantitative information on the fraction of rBC associated with HOA and OOA. For these mobile data, we chose a two-factor solution with rotational forcing parameter fPeak = 0.2 ($Q/Q_{exp} = 0.98$), yielding a hydrocarbon-like OA (HOA) component combined with rBC, hereafter HOA + rBC, and an oxygenated OA (OOA) component combined with rBC (hereafter OOA + rBC). A detailed summary of key diagnostic plots of the PMF results and a discussion of the factor solution choices are reported in supplemental information (Figure S3 and related text). Figure 4 presents the high resolution mass spectral profiles (MS) and mass-weighted pie charts of the ion components for the two PMF factors HOA + rBC (Figure 4a) and OOA + rBC (Figure 4b). The elemental composition (H/C, O/C, N/C) and the OM/OC calculated using the standard AMS data analysis code (Aiken et al. 2007) are also reported.

The rBC is represented by the ion family C_x^+. From the MS, we infer that most of the rBC signal (~90%) resides between C_1^+ (m/z = 12) and C_5^+ (m/z = 60), consistently with previous laboratory measurements (Onasch et al. 2012). The C_3^+ cluster (m/z = 36) is the most abundant one, followed by C_1^+ (C_1^+:C_3^+ = 0.6) and C_2^+ (C_2^+:C_3^+ = 0.3). The HOA + rBC spectrum is dominated by the characteristic $C_xH_{2y-1}^+$ and $C_xH_{2y+1}^+$ ion pattern, with the hydrocarbon like ions $C_3H_7^+$ (m/z = 43), $C_4H_7^+$ (m/z = 55), and $C_4H_9^+$ (m/z = 57) being the dominant peaks. The rBC accounts for ~50% of the total HOA + rBC component mass concentration, whereas the remaining HOA + rBC mass is dominated by ions in the $C_xH_y^+$ family. The HOA + rBC spectrum is overall consistent with previously reported ambient HOA spectra (Zhang et al. 2005b; Sun et al. 2011a; Ng et al. 2011b). The slightly larger amount of CO_2^+ signal at m/z = 44 relative to m/z 43 (even after correction for the contribution of gas phase CO_2) could be SP-AMS specific, and arise from the fragmentation of refractory oxygenated soot compounds that vaporize in the SP laser at temperatures higher than 600°C (Onasch et al. 2012). Consistently, the average O/C ratio calculated for the HOA + rBC component (0.12) is slightly higher than what found for HOA factors determined via PMF analyses of HR-AMS spectra acquired near the LIE during the same day and time frame (Sun et al. 2012). The OOA + rBC spectrum is dominated by CO_2^+ at m/z = 44. $C_2H_3O^+$ at m/z = 43 and CHO^+ at m/z = 29 are the second and third most abundant peaks. Ions of both $C_xH_y^+$ and $C_xH_yO_1^+$ families are present above m/z = 50. The pie chart indicates that the rBC mass in this case is only 20% of the total OOA + rBC component, and that the remaining coating mass is almost equally distributed among the $C_xH_y^+$, $C_xH_yO_1^+$, and $C_xH_yO_{>=1}^+$ ion families. The average H/C and O/C values for the OOA + rBC component are 1.43 and 0.56, respectively, in good agreement with published data for total OOA from worldwide locations (Jimenez et al. 2009; Ng et al. 2010). Comparison of our PMF factors with literature HOA and OOA MS obtained by a standard AMS (Ng et al. 2011b) yields r^2 of 0.9 (slope = 0.83) for HOA + rBC and r^2 of 0.8 (slope = 0.76) for OOA + rBC, respectively. We also calculated r^2 between the two PMF factors and gas-phase tracers, particle number and BC concentrations (Table 1). HOA + rBC correlates best with CO_2, BC, and NO_x (r^2 = 0.35, 0.5, and 0.6, respectively) whereas OOA + rBC shows no correlation with the traffic-related species, and only a weak correlation with O_3.

The spatial-temporal gradients of the HOA + rBC and OOA + rBC factors as well as of their ratio are shown in Figure 5 for the transits downwind of the LIE.

The HOA + rBC varies like the other traffic related species. A similar result was found for the Somerville study using a standard AMS (Canagaratna et al. 2010). Conversely, OOA + rBC does not change with either distance or time, and therefore, it can be interpreted as an oxidized ORG coating associated with "aged" background rBC rather than with freshly emitted rBC. The HOA + rBC/OOA + rBC ratio shows a spatial and temporal trend that is qualitatively similar to HOA + rBC, indicating that HOA-like material is directly associated with traffic emissions and, in the first 200 m downwind of the LIE, it dominates the ORG coating of rBC particles (which are also the least coated according to the cPM/rBC trends of Figure S2).

Note that the SP-AMS mass concentrations reported in this article are multiplied by a factor of 9 based on the correlation between the rBC measured by the SP-AMS and the BC measured by MAAP. Figure 6a, shows such correlation for both the gradient experiments of 28 July and 31 July as well as for the measurements at the QC site.

The slope of the fit to the data (~0.11) indicates that during the QC campaign the SP-AMS reported about time times less BC mass than the MAAP. This number effectively represents the collection efficiency (CE) of the SP-AMS during the QC deployment. The larger size cut of the MAAP instrument (2.5 μm,

TABLE 1
The r^2 obtained between the SP-AMS based PMF factors HOA + rBC and OOA + rBC and external tracers for the gradient measurements of 28 July 2009

	r^2		r^2
HOA vs. BC[a]	0.5	OOA vs. BC[b]	0.01
HOA vs. CO_2	0.35	OOA vs. CO_2	0.05
HOA vs. NO_x	0.6	OOA vs. NO_x	0.03
HOA vs. pp[b]	0.25	OOA vs. pp[c]	0.01
HOA vs. O_3	0.02	OOA vs. O_3	0.2

[a]BC from MAAP measurements
[b]Particle number concentration (p cm^{-3}) from CPC.

Downloaded by [Institute Of Atmospheric Physics] at 20:09 13 July 2012

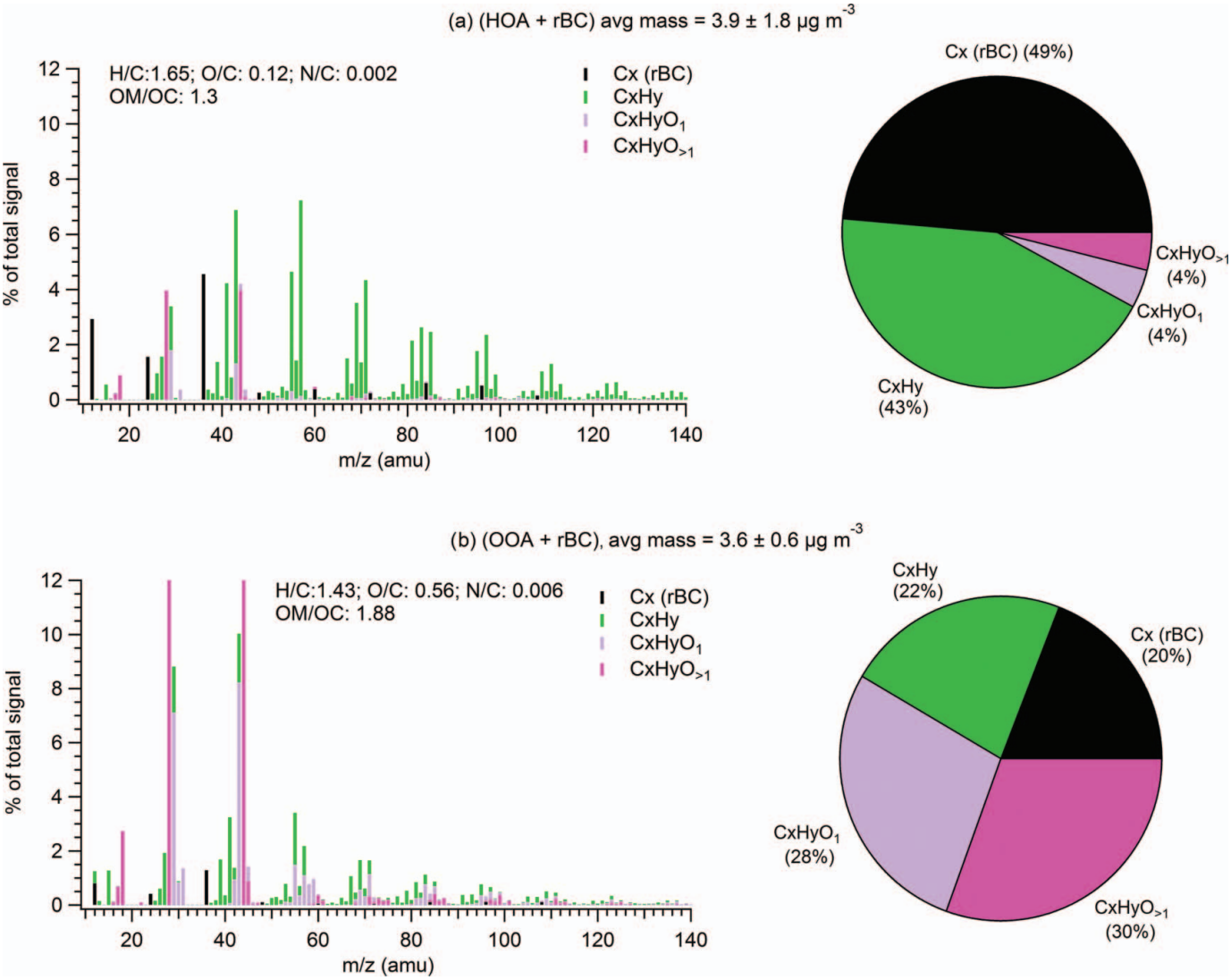

FIG. 4. Results of the PMF analyses performed on the mobile SP-AMS data (combined ORG and rBC matrices) of 28 July 2009, 0430–0845 EDT. Mass-spectra and mass-weighted pie charts, colored by ion families, are shown for HOA + rBC and OOA + rBC. rBC is mostly associated with HOA-like aerosol. The HOA + rBC coating mass is dominated by CxHy ions whereas the OOA + rBC coating mass is equally split among the CxHy, $CxHyO_1$, and $CxHyO^{>1}$ ion families.

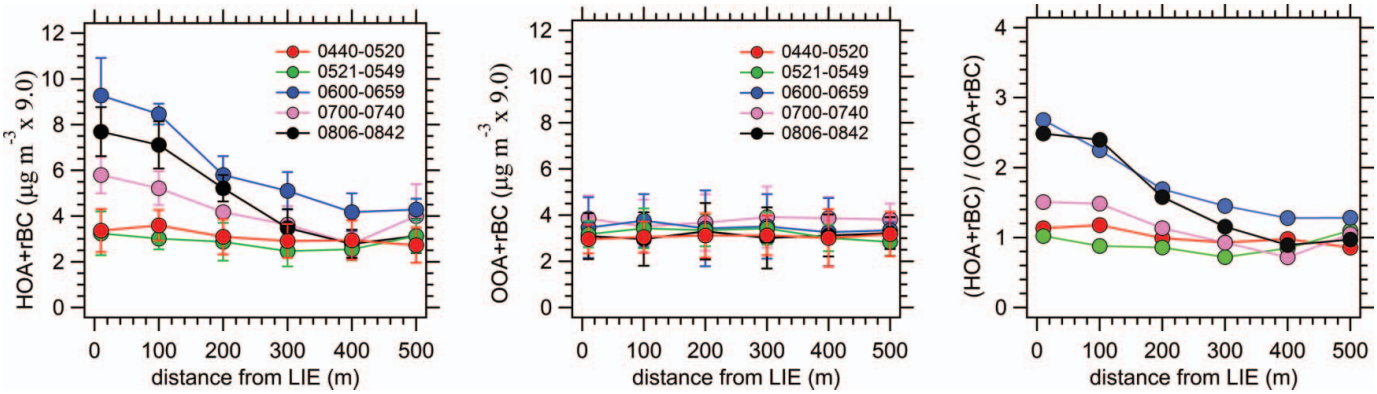

FIG. 5. Spatial-temporal gradients of HOA + rBC and OOA + rBC. HOA + rBC has the a similar trend as the other traffic related species (NO, rBC, CO_2), whereas OOA + rBC trends are flat. The ratio between the two factors suggests that HOA + rBC dominates PM_1 directly downwind of the LIE (<200 m), whereas OOA + rBC is not directly associated with traffic and it is present in background PM.

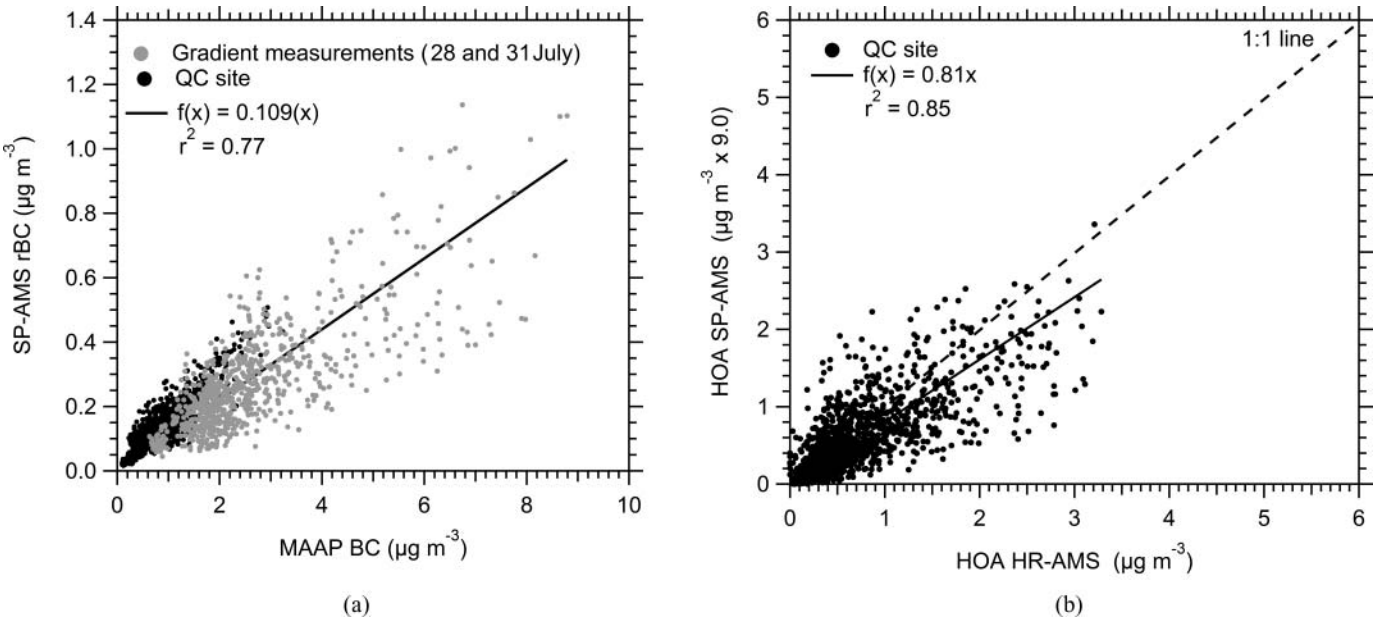

FIG. 6. (a) Correlation plot of SP-AMS rBC and MAAP BC for the QC site data (black) and gradient measurements of 28 July and 31 July 2009 (grey). The average regression slope of the fit to the data (0.109) defines the SP-AMS *CE* for the QC study. (b) Correlation between SP-AMS HOA (with *CE* applied) and HR-AMS HOA measurements at the QC site. The fit to the data indicates that most of the HOA (80%) is associated with rBC.

Downloaded by [Institute Of Atmospheric Physics] at 20:09 13 July 2012

determined by the URG cyclone) compared to the SP-AMS (0.8 μm, determined by the aerodynamic lens) is expected to have a negligible contribution to the observed mass difference, since previous studies have shown that the bulk of BC mass resides in the submicron range (Cozic et al. 2007; Harrison et al. 2011). Rather, we believe that CE for the SP-AMS during the QC study was likely affected by a nonoptimal laser-to-particle beam vertical alignment, which ultimately governs the fraction of particles that cross the laser. Because the width of the 1064 nm laser is less than the average particle beam width, substantial losses of small and non-spherical particles can occur in the SP-AMS due to beam divergence, if particle and laser beams do not perfectly overlap. These technical aspects, including best practices for maximizing the laser-to-particle alignment with respect to the ion region extraction in the SP-AMS, are extensively addressed in Onasch et al. (2012). During the QC study, the narrow size range of rBC-containing particles sampled (most of rBC mass was around 100 nm D_{va}) did not allow to obtain useful information on any possible size-dependent CE, which are currently being explored with other SP-AMS datasets.

3.3. Comparison Between SP-AMS and HR-AMS Data at the QC Site

In this section, we present a comparison of the SP-AMS and HR-AMS stationary data. Figure 6b shows the comparison between the primary hydrocarbon-like organic aerosol (HOA) mass concentrations extracted with PMF analyses for both the SP-AMS and the SUNY HR-AMS data (Sun et al. 2011a) collected at the QC site. In this case, the PMF analysis of the SP-AMS was performed only on the ORG component to extract an HOA factor that could be directly compared with the SUNY HR-AMS PMF results. The key diagnostic plots for evaluating the PMF analysis performed on the SP-AMS QC site data are reported in supplemental material (Figures S4 and S5 and related text). With the SP-AMS HOA corrected for a CE = 0.11 according to Figure 6a, we obtain a regression slope of 0.81 ($r^2 = 0.85$) for the HOA comparison with the HR-AMS, indicating that most of the measured HOA is associated with rBC particles. Such result is expected based on the fact that primary organic material emitted from combustion sources is supposed to be directly associated with rBC (Zhang et al. 2005d).

Figure S6 shows correlation plots between the SP-AMS coating species ORG-HOA (total ORG minus the HOA component shown in Figure 6b), SO_4, NO_3, and NH_4 measured at the QC site and the same species obtained from the co-located SUNY HR-AMS. The unique combination of the two datasets allows an estimate of the fraction of the NR-PM_1 (measured by HR-AMS) that is associated with rBC (measured by SP-AMS), that is, 20, 23, 30, and 35% for SO_4, NH_4, NO_3, and ORG-HOA, respectively. The fact that SO_4 is the species the least associated with rBC is consistent with previous results from standard AMS data (Zhang et al. 2005c) showing that SO_4 correlates with the most oxidized component of the aerosol, more likely to be found in aged NR-PM_1 rather than in the coating material associated with rBC.

3.4. SP-AMS Size Distribution Measurements of Traffic Emissions

Figure 7a, shows the chemically resolved average pToF size distributions ($dM/d\log_{10}d_{va}$) and composition pie charts

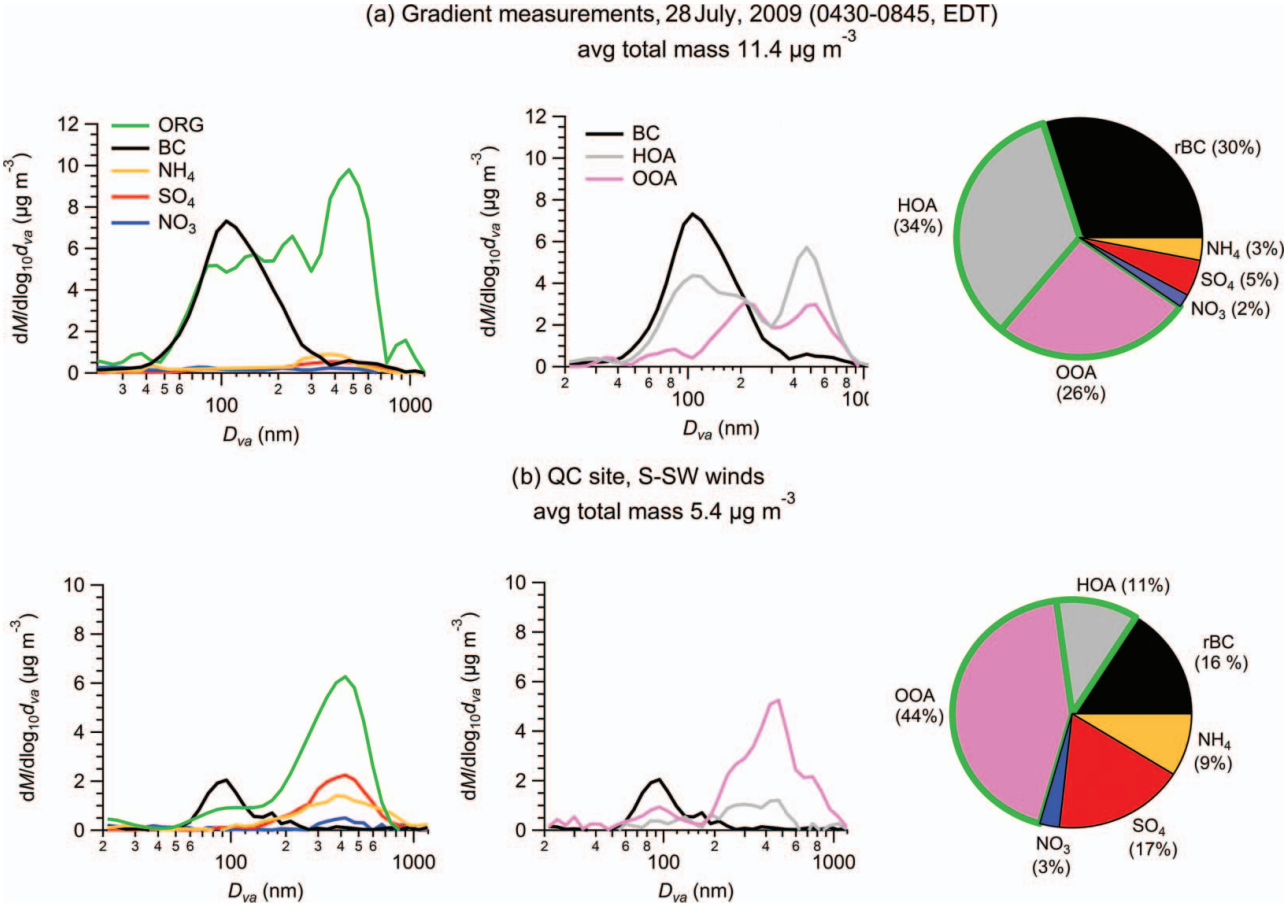

FIG. 7. Chemically resolved, mass normalized pToF size distributions and composition pie charts for (a) the gradient measurements downwind and upwind of the LIE on 28 July 2009 (04:30–08:45 EDT) and (b) SP-AMS measurements at the QC site (upwind of the LIE). The pToF size distributions of HOA and OOA (from m/z 44 and m/z 57 tracers normalized to HOA and OOA mass, respectively) are also shown. The rBC mass is concentrated around $D_{va} \sim 100$ nm ("fresh soot" mode). HOA dominates the 500 nm D_{va} mode downwind of the LIE. Under S-SW winds, the pToF at the QC site is dominated by accumulation mode ORG (mainly OOA) and SO_4 coatings. The pToF traces are smoothed using binomial algorithm.

for the gradient measurements of 28 July 2009 (04:30–08:45 EDT, data including both downwind and upwind transits). Similarly to Cross et al. (2010), we use the particle time-of-flight (pToF) of m/z 36 from unit mass resolution (UMR) data as a proxy for the rBC size distribution because the C_3^+ at m/z 36 is the strongest carbon cluster signal in the rBC MS (Figure 4), and the interference from particle-phase chlorine at m/z 36 is generally less than, for example, the SO_4 interference at m/z 24 (C_2^+). The pToF size distribution traces are normalized to the mass concentrations of the corresponding species obtained from the high-resolution analysis.

The rBC mass is concentrated around $D_{va} \sim 100$ nm ("fresh soot" mode). rBC and ORG each contribute approximately 50% to the total measured mass below 300 nm D_{va}. These SP-AMS data confirms that the particle mode detected by standard AMS at $D_{va} \sim 110$ nm during previous studies in similar environments (Canagaratna et al., 2004, 2010; Schneider et al., 2005; Zhang et al., 2005a–d) is the vehicles exhaust "fresh soot" mode. The weaker rBC mode ("accumulation soot") centered at ~500 nm D_{va} is instead more heavily coated with ORG. At these large D_{va} values, rBC represents only ~5% of the total mass whereas, on average, ORG contributes 90% of the total mass (the remaining 5% is represented by the sum of SO_4, NO_3, and NH_4).

The middle panel of Figure 7a shows the size distributions of HOA and OOA obtained using the tracer-based method described in Zhang et al. (2005b, d), that is, using, respectively, the UMR pToF signals at m/z 44 (CO_2^+) and m/z 57 (mainly $C_4H_9^+$ in this case based on HR analysis) normalized to HOA and OOA mass loadings. The pie chart provides a comprehensive summary of the PM_1 composition measured during the 5 h drive, and shows that rBC and HOA are the most abundant components in near source conditions. HOA has a bimodal distribution, with one mode correlating with the rBC "fresh soot" at ~110 nm D_{va} and a second mode contributing significantly to the ORG coating at ~500 nm D_{va}. The difference in D_{va} between fresh and accumulation rBC modes is consistent with the fresh exhaust soot particles having a nonspherical core as well as a different chemical composition and density than the

Downloaded by [Institute Of Atmospheric Physics] at 20:09 13 July 2012

Downloaded by [Institute Of Atmospheric Physics] at 20:09 13 July 2012

accumulation soot, possibly more aged, particles (Canagaratna et al. 2004). OOA does not correlate with the 110 nm D_{va} rBC mode and it is mostly detected above 200 nm D_{va}. Such interpretation is consistent with the OOA being mostly associated with background, aged soot. The relatively large HOA fraction in the 500 nm D_{va} mode could have some contribution from fresh exhaust particles condensing onto (or coagulating with) pre-existing accumulation mode soot, but it could also reflect direct traffic emissions from the occasional re-entrainment of particles deposited on exhaust-line surfaces (Kittelson 1998; Canagaratna et al. 2004). During the same time frame, Sun et al. (2012) reported similar pToF size distributions from the SUNY standard HR-AMS stationed 30 m upwind of the LIE. Consistently with our result, the HR-AMS pToF size distributions showed a primary emission mode at D_{va} ~100 nm dominated by HOA and a second mode at D_{va} ~500 nm dominated by OOA. Despite the different location of the two AMSs with respect to the LIE emissions, the HOA mass reported by SP-AMS and HR-AMS is in very good quantitative agreement at both 110 and 500 D_{va} under "high traffic conditions" (see Figure 5b of Sun et al. 2012). However, the SP-AMS (with CE applied) detects only 1/3 of the OOA and 1/20 of the SO_4 mass compared to what reported by the HR-AMS at the 500 nm D_{va} mode. This suggests (and somewhat confirms) that the majority of the accumulation mode PM_1 is non-refractory OOA and SO_4, not associated with a rBC core, and therefore, not detected by the SP-AMS in the laser-only configuration.

In order to put near-roadway results more in context with average ambient data, Figure 7b, shows chemically resolved pToF size distributions and composition pie charts of SP-AMS measurements at the QC site for periods characterized by S–SW winds (i.e., same meteorological conditions encountered during the gradient experiments). Similarly to Figure 7a, the rBC pToF is centered at ~100 nm D_{va}. However, the average rBC mass in this size range is much lower than the average rBC mass measured downwind of the LIE (i.e., 2 μg m^{-3} vs. 7 μg m^{-3}, respectively), and the pToF is dominated in mass by ORG, SO_4, and NH_4 coating material centered at ~500 nm D_{va}. Moreover, the ORG mass at 500 nm D_{va} is mostly OOA rather than HOA (as also highlighted in the composition pie charts). The differences in PM composition as well as in distribution of rBC and coating material components among the two D_{va} modes between the QC site and the near-roadway conditions highlight the differences in PM sources upwind and downwind of the LIE, respectively. Finally, it is worth noticing that the average pToF and fractional composition of the NR-PM_1 reported by the HR-AMS for the entire three-week period at the QC site (see Figure 6a of Sun et al. 2011a) compares well with the average SP-AMS pToF of Figure7b, which is representative of the 3 weeks QC study based on the prevailing wind direction (S–SW ~70% of the times).

3.5. Characterization of Single Vehicles

During the QC study, the AML was also deployed in "chase" mode similar to Canagaratna et al. (2004), that is, each vehicle was closely followed at a distance of 5 m or less, and usually for 2–5 min while driving through city traffic. Under these conditions, the typical average speed of both AML and chased vehicles was ~20 km h^{-1}, with slight variations of speed and engine loads occurring due to traffic dynamics (e.g., stopping/accelerating). Targeted vehicles were randomly chosen among several types of NYC Metropolitan Authority Transit (MTA) buses running standard diesel-powered and hybrid engines as well as using alternative fuel such as compressed natural gas (CNG). Between five and ten single chases were performed for MTA buses, non-MTA buses and other HD and medium-duty (MD) vehicles, including school buses. Here, we report the chemically resolved pToF, high-resolution MS and mass-weighted composition pie charts for two MTA buses and a diesel (HD) vehicle (Figure 8).

The first MTA bus used a standard diesel engine, while the second MTA bus, labeled "clean technology," was equipped with a Continuously Regenerating Technology (CRT^{TM}, Johnson-Matthey trademark) trap system, that is, a catalyzed diesel particulate filter (DPF) that in recent years has commonly been implemented in diesel engines to meet the 2007 standards for PM emission control (EPA 2002). The contribution of the background aerosol has been subtracted from both pToFs and MS. The mass loadings measured for rBC and ORG coating material are reported for each specific case. Higher PM_1 emissions (here defined as the sum of SP-AMS rBC and ORG coating) are observed for the diesel vehicles compared to the CRT bus. The pToF of both HD vehicle and standard MTA diesel bus shows one rBC mode centered at D_{va} ~100 nm, coated with ORG only. The corresponding pie charts indicate that those emissions are dominated by rBC, which represents approximately 58% of the total carbon mass measured by the SP-AMS. The dominance of rBC (in mass) in these diesel vehicle emissions is qualitatively consistent with a large pool of literature data generally showing a much larger fraction of EC compared to OC (in % of fine-particle mass) for diesel-powered vehicles probed in chassis dynamometer studies (Schauer et al. 1999), tunnel studies (Ban-Weiss et al. 2007), and real-world conditions (Shah et al. 2004). The MS show that for both the HD vehicle and the MTA diesel bus almost all the ORG coating (~42% of the remaining carbon mass) is represented by hydrocarbon-like ions of the C_xH_y family, and it is likely dominated by condensed lubricating oil (Canagaratna et al. 2004). The oxygenated fraction ($C_xH_yO_1$ and $C_xH_yO_{>1}$) accounts for less than 0.1% of the ORG coating mass found in these diesel exhaust plumes. The CRT bus emissions show a strikingly different composition, with rBC representing only the 27% of the total carbon mass detected by the SP-AMS. In addition, the pToF shows a considerably weaker rBC mode at 100 nm D_{va}, and no clearly interpretable ORG pToF. Despite the different proportion of rBC to ORG mass, the C_xH_y ions dominate the MS of the CRT bus emission as well. In fact, the MS features for all of these vehicles types are typical of an HOA aerosol, a result somehow expected based on the nature of the emissions. Just as observed in the HOA + rBC spectrum of

Downloaded by [Institute Of Atmospheric Physics] at 20:09 13 July 2012

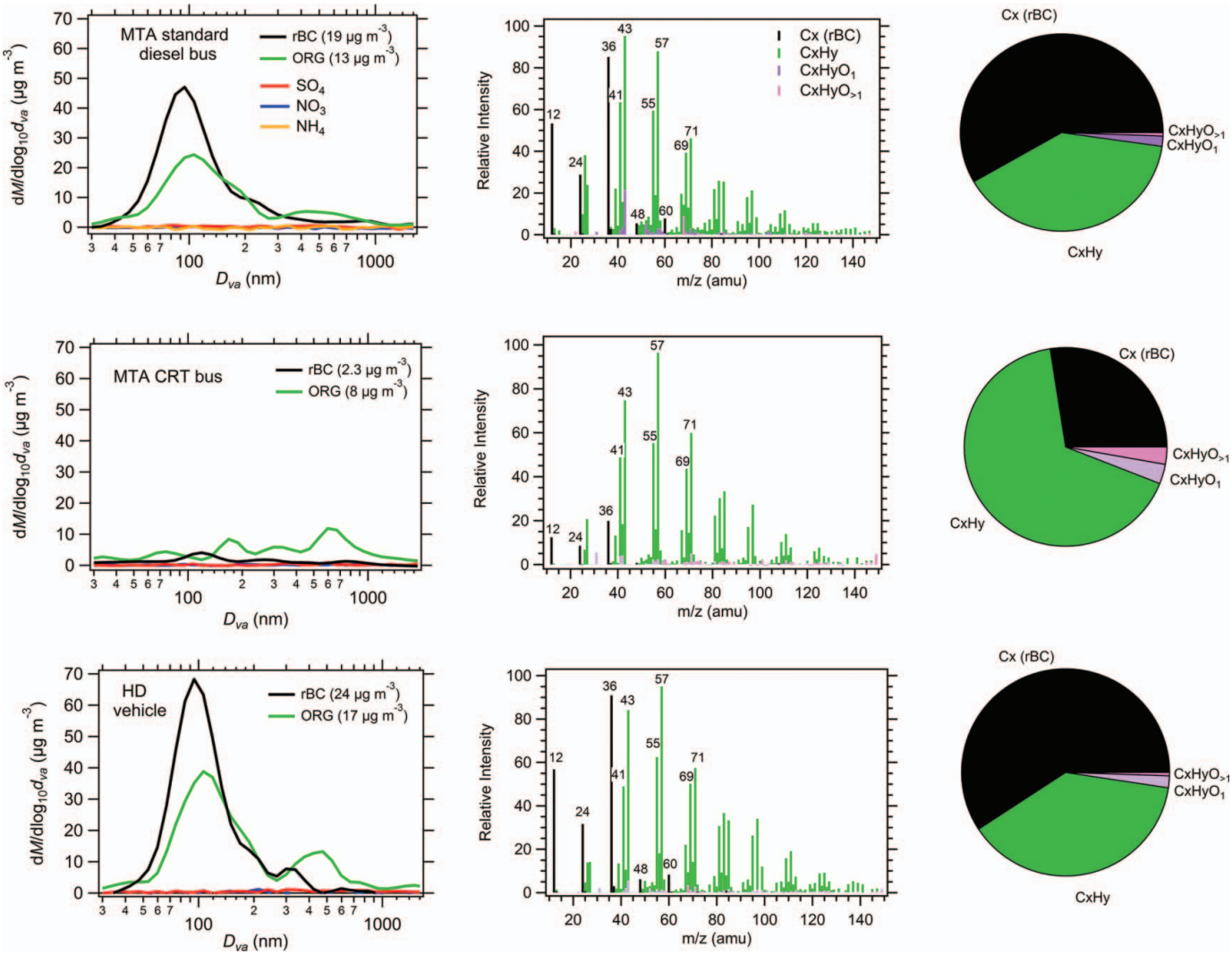

FIG. 8. Chemically resolved pToFs, high resolution mass spectra (MS), and mass-weighted composition pie charts of single vehicle emissions sampled in "chase" mode, for a standard diesel engine MTA bus, a CRT bus and a HD vehicle (diesel truck). The contribution of the background aerosol has been subtracted from both pToF and MS. The average mass loadings of rBC and ORG are reported. The pToF traces are normalized to mass and smoothed using a binomial algorithm. The rBC mode is centered at ~100 nm D_{va}. The emissions from the diesel MTA bus and HD vehicle are dominated by rBC, whereas the CRT bus has higher amount of ORG coating relative to rBC mass. All MS are typical of an HOA aerosol.

Figure 5a, the C_1^+, C_2^+, and C_3^+ carbon clusters account for ~90% of the rBC signal in these single vehicle plumes. The C_3^+ cluster is the most abundant, and the ratios C_1^+:C_3^+ and C_2^+:C_3^+ are 0.6 and 0.3, respectively. ORG is dominated by $C_3H_7^+$ (m/z = 43), $C_4H_7^+$ (m/z = 55), $C_4H_9^+$ (m/z = 57), and $C_5H_{11}^+$ (m/z = 71). Similarly to the CRT bus, the emissions from CNG and hybrid/electric MTA buses sampled in chase mode (data not shown) were also very low in rBC. It is worth noticing that other rBC coating species (SO_4, NH_4, and NO_3) do not contribute significantly to the emissions of these vehicles (i.e., only ORG is associated with the primary soot mode). This result is consistent with the negligible amount of SO_4 particles observed in the 100 nm D_{va} mode during chases of diesel vehicles using a standard AMS (Canagaratna et al. 2004). Table S1 shows the r^2 values between MS (ORG only) of both MTA buses with ambient diesel exhaust, laboratory generated lubricant oil and pure diesel fuel MS obtained by standard AMS (Canagaratna et al. 2004). The highest r^2 values are found between the standard MTA bus and diesel exhaust, and between the CRT MTA bus and lubricating oil.

3.6. Estimates of EI

Here, we discuss the EI values calculated for single vehicles and on-road conditions sampled during the QC study. Values are reported for rBC (EI_{rBC}), particle number (EI_{pp}), and for optical measurements, that is, optical extinction measured by CAPS (EI_{ext}) and optical absorption measured by MAAP (EI_{abs}). The EI_{rBC} are mostly based on the 1s MAAP rBC data, as "fast"

TABLE 2

EI of gas phase and particle species measured for specific vehicles during "chase" studies (the number of chased vehicles indicated in parentheses). Average EI values for average on-road conditions are also reported. EI units are g kg^{-1} of fuel burnt (in CO_2 equivalents) for BC, $kg^{-1} \times 10^{15}$ for particle number, and $m^2\ kg^{-1}$ for the optical data

	EI BC (g kg^{-1})	EI PP ($kg^{-1} \times 10^{15}$)	EI ext ($m^2\ kg^{-1}$)	EI abs ($m^2\ kg^{-1}$)
On-road conditions				
Mixed HD and LD	0.46 ± 0.016	$5.3 \pm 1.05e+5$	3.4 ± 0.01	1.5 ± 0.13
LD dominated	0.04 ± 0.005	$9.0 \pm 0.47e+5$	1 ± 0.026	0.45 ± 0.034
Single Chases				
HD (8)	0.88 ± 0.1	1.25 ± 0.45	7.4 ± 0.77	6 ± 0.78
MD (5)	0.2 ± 0.08	0.82 ± 1.6	0.83 ± 0.03	0.44 ± 0.03
School buses (3)	0.6 ± 0.18	0.8 ± 0.1	5.6 ± 0.3	3.15 ± 1.15
MTA standard diesel (7)	0.56 ± 0.07	0.92 ± 0.1	6.4 ± 0.38	3.2 ± 0.28
MTA CNG (3)	0.098 ± 0.02	1.57 ± 0.2	0.87 ± 0.09	0.68 ± 0.14
MTA Hybrid (4)	0.017 ± 0.002	0.09 ± 0.01	0.4 ± 0.013	0.13 ± 0.01
MTA CRT (5)	0.005 ± 0.001	1.87 ± 0.2	1.2 ± 0.02	0.03 ± 0.007

Downloaded by [Institute Of Atmospheric Physics] at 20:09 13 July 2012

SP-AMS data were not available for every chase (when both available, the EI_{rBC} from SP-AMS and MAAP compared within 5%). Similarly, EI values for NO_x are not reported for the chases because the NO_x monitor was operated in a way that did not provide the necessary fast time resolution for accurate peak analysis and quantitative EI calculations.

Table 2 summarizes the average EIs obtained for each vehicle type. The HD and medium-duty (MD) vehicles have the highest BC and particle optical property EI among the single chased vehicles. Similarly, we find significantly higher EI_{rBC}, EI_{ext}, and EI_{abs} for the standard MTA buses compared to CNG, CRT, and hybrid/electric (Orion Bus Industries) ones. This result is consistent with the SP-AMS pToFs of Figure 8 showing higher rBC mass in diesel buses exhaust compared to CRT, CNG, and hybrid/electric buses. Particle number emission factors (EI_{pp}) were instead higher for the sampled CNG and CRT buses. While these results might not be statistically significant due to the limited number of chased vehicles, they are qualitatively consistent with previous studies. For example, the average EI_{rBC}, EI_{ext}, and EI_{abs} values that we obtain for standard MTA buses and HD vehicles compare well to literature values of EI for diesel emissions (Ban-Weiss et al. 2007, 2009; Strawa et al. 2010). Chassis dynamometer based studies have reported a general trend for lower emissions of refractory PM (i.e., soot) but high emissions of semivolatile organic PM and, under some circumstances, of nucleation mode particles of $D_m < 30$ nm in diesel vehicles retrofitted with CRT technology compared to regular diesel vehicles (Kittelson et al. 2008; Biswas et al. 2009, and references therein). Recent studies on emissions from diesel and CNG buses (Jayaratne et al. 2008) showed that the CNG buses emit 10–100 times less accumulation mode PM than diesel ones, but a considerably higher number of ultrafine ($D_m < 100$ nm) volatile particles, consistent with our high EI_{pp}. Consistently, Canagaratna et al. (2004) reported that in-use NYC MTA diesel buses have much larger particulate EI (around 0.2 g NR-PM_1/kg fuel) than those fueled by CNG (<0.1 g NR-PM_1/kg fuel) using a standard AMS. Finally, it is worth pointing out that NO_x EI for several standard diesel, CNG, CRT, and hybrid/electric MTA buses were measured with high accuracy in a previous campaign in Queens, NYC, with a ARI tunable infrared laser differential absorption spectrometer (TILDAS) deployed on the AML (Shorter et al. 2005). That study showed that NO_x emissions from CNG buses (35 g kg^{-1}) were comparable to those from standard diesel buses (~38 g kg^{-1}), but were much lower for hybrid/electric buses (~15–20 g kg^{-1}). In addition, CRT buses were found to have higher NO_2/NO_x ratio (30%) compared to diesel buses (10%), which mostly emit NO.

Table 2 also presents EI_{rBC} (in this case obtained using SP-AML data), EI_{pp}, EI_{ext}, and EI_{abs} values for average fleet conditions, obtained while driving the AMS in mixed (~60% HD/MD, 40% LD) and LD-dominated (10% HD/MD, ~90% LD) traffic. In both cases, the traffic was very sustained, with an average vehicle speed of 15–20 km h^{-1} for both AML and surrounding vehicles. We observed higher EI_{rBC}, EI_{ext}, and EI_{abs} in mixed traffic, compared to when the AML was driving in LD-dominated traffic. For these on-road conditions, we were able to estimate an EI for NO_x of 4.0 ± 0.08 g kg^{-1} in LD-dominated and 8.4 ± 0.08 g kg^{-1} in mixed traffic. The EI_{rBC} estimated by the SP-AMS was 0.46 g kg^{-1} for mixed traffic and 0.04 g kg^{-1} for LD-dominated conditions. Despite the possible variety of driving speeds and engine load conditions of the sampled vehicles, these results are consistent with previous EI_{BC} reported for comparable traffic conditions near roadways where EI for EC was obtained from filter based techniques (Ning et al. 2008). Similarly, our EI_{BC}, EI_{ext}, and EI_{abs} values reported for LD-dominated traffic compare well with results from tunnel studies during which LD vehicles were sampled in a dedicated bore (Ban-Weiss et al. 2008, 2009; Strawa et al. 2010).

Downloaded by [Institute Of Atmospheric Physics] at 20:09 13 July 2012

Finally, we report average EI based on the SP-AMS data collected during the gradient measurements. Figure S7 presents the correlation plots for background-subtracted values of rBC and HOA (μg m^{-3}) versus CO_2 (ppmv) for all the transits during the 04:30–08:45 time frame. The slopes of the fits to the data (multiplied by $f_{\text{fuel}} = 1.76$ according to Equation (1) provides average values of $EI_{rBC} = 0.09$ g kg^{-1} and $EI_{HOA} = 0.12$ g kg^{-1}. Points with larger (and more variable) excess rBC and HOA values correspond to transits closest to the LIE. For HOA, this result is very similar to what obtained from previous standard AMS measurements downwind of major roadways (Canagaratna et al. 2010). The EI_{rBC} of ~0.1 suggest emissions dominated by LD vehicles during rush hours, consistent with the estimate of only ~12% of the LIE traffic being represented by HD vehicles according to the manual counting performed during the same time frame (Sun et al. 2012).

4. SUMMARY

We presented mobile measurements of traffic-related emissions performed nearby a major highway (LIE) in NYC during morning rush hours. The AML, equipped with state-of-the-art instrumentation, provided the spatial and temporal evolution of both gaseous and particle phase pollutants, as well as the size distribution, optical properties and chemical composition of the traffic related PM. During this study, the recently developed soot particle aerosol mass spectrometer (SP-AMS) was deployed for the first time outside the laboratory and provided direct chemical characterization and quantification of rBC-containing particles. Up to 6 μg m^{-3} of rBC were measured on 28 July and 31 July during transits 10 m downwind of the LIE under stagnant conditions (wind speed <2 m/s); particle number concentrations varied between 0.5 and 1×10^5 p cm^{-3}, with 90% of the particle number residing in the ultrafine range ($D_m < 60$ nm). In agreement with previous similar studies, pollutant concentrations (CO_2, NO_x, NO, rBC) were found to drop up to 50% within 150 m downwind of the highway due to dilution effects. Although near-highway personal exposure to traffic pollution can vary greatly depending on specific meteorological conditions, these results confirm that communities living adjacent to high traffic roads are often exposed to concentrations of pollutants that are typically 20–50% higher than 200 m or more away from source. Therefore, long-term measurements of pollutants near highways are needed to better characterize how different meteorology conditions, traffic regimes and vehicle types might affect public health.

Chemically resolved size distributions of traffic-related particles (pToF) measured by the SP-AMS were dominated by a mode peaking at ~100 nm D_{va}, slightly coated by organic material (rBC = 50% of the total measured mass) and by a accumulation mode at ~500 nm D_{va} containing soot more heavily coated with organics and sulfate (rBC = 5% of the total measured mass), representing "background" PM. These SP-AMS measurements support the interpretation of previous standard AMS measurements of nonrefractory PM collected directly downwind similar emission sources, confirming that the particle mode detected at D_{va} ~100 nm is the "fresh soot mode." Detailed spectral analysis of the emissions sampled near the LIE indicates that the organic coating of the rBC particles is represented by HOA material (mostly C_xH_y ions), whereas OOA (mostly $C_xH_yO_1$ ions) shows little influence from traffic emissions and it mainly exists in the accumulation mode ("background" soot). PMF analyses performed on the near-roadway data indicate that the fraction of rBC associated with HOA is larger than the fraction associated with OOA (50% and 25% of the total HOA + rBC and OOA + rBC mass respectively). For the stationary measurements at the QC site, the comparison of SP-AMS-based rBC coating species and HR-AMS-based NR-PM_1 represent the first direct assessment of evaluating the fraction of rBC associated with NR-PM_1. We find that ORG represents the largest fraction of the coating PM associated with rBC (35%). However, for the average ambient conditions (not directly influenced by traffic emissions) the OOA fraction associated with rBC is larger than the HOA fraction. Finally, the "chase" studies performed on single vehicles and New York City MTA buses confirm significant differences in rBC emissions between standard diesel engines (dominated by rBC) vs. buses using alternative fuels and/or equipped with PM control technologies (dominated by ORG).

REFERENCES

Aiken, A. C., DeCarlo, P. F., and Jimenez, J. L. (2007). Elemental Analysis of Organic Species with Eelectron Ionization High-Resolution Mass Spectrometry. *Anal. Chem.*, 79:8350–8358.

Ban-Weiss, G. A., Lunden, M. M., Kirchstetter, T. W., and Harley, R. A. (2009). Measurement of Black Carbon and Particle Number Emission Factors from Individual Heavy-Duty Trucks. *Environ. Sci. Technol.*, 43:1419–1424.

Ban-Weiss, G. A., McLaughlin, J. P., and Harley, R. A. (2008). Carbonyl and Nitrogen Dioxide Emissions from Gasoline and Diesel-Powered Motor Vehicles. *Environ. Sci. Technol.*, 42:3944–3950.

Ban-Weiss, G. A., McLaughlin, J. P., Harley, R. A., Lunden, M. M., Kirchstetter, T. W., Kean, A. J., et al. (2007). Long-Term Changes in Emissions of Nitrogen Oxides and Particulate Matter from On-Road Gasoline and Diesel Vehicles. *Atmos. Environ.*, 42:220–232

Beckerman, B., Jerrett, M., Brook, J. R., Verma, D. K., Arain, M. A., and Finkelstein, M. M. (2008). Correlation of Nitrogen Dioxide with Other Traffic Pollutants near a Major Expressway. *Atmos. Environ.*, 34:51–59.

Biswas, S., Verma, V., Scahuer, J. L., Cassee, F. R., Cho, A. R., and Sioutas, C. (2009). Oxidative Potential of Semi-Volatile and Non-Volatile Particulate Matter (PM) from Heavy-Duty Vehicles Retrofitted with Emission Control Technologies. *Environ. Sci. Technol.*, 43:3905–3912.

Brugge, D., Durant, J. L., and Rioux, C. (2007). Near Highway Exposure to Motor Vehicle Pollutants: Emerging Evidence of Cardiac and Pulmonary Health Risks. *Environ. Health*, 6(23): DOI: 10.1186/1476-069X-6-23. Available online at: http://www.ehjournal.net/content/6/1/23,2007.

Brunekreef, B., Janssen, N. A., de Hartog, J., Harssema, H., Knape, M., and vanVliet, P. (1997). Air Pollution from Truck Traffic and Lung Function in Children Living Near Motorways. *Epidemiology*, 8:298–303.

Bukowiecki, N., Lienemann, P., Hill, M., Furger, M., Richard, A., Amato, F., et al. (2010). PM10 Emission Factors for Non-Exhaust Particles Generated

by Road Traffic in an Urban Street Canyon and Along a Freeway in Switzerland. *Atmos. Environ.*, 44:2330–2340.

Chan, E., and Vet, R. J. (2009). Background Ozone Over Canada and the United States. *Atmos. Chem. Phys.*, 10:8629–8647.

Canagaratna, M. R., Jayne, J. T., Ghertner, D. A., Herndon, S. C., Shi, Q., Jimenez, J. L., et al. (2004). Chase Studies of Particulate Emissions from In-Use New York City Vehicles. *Aerosol Sci. Technol.*, 38:555–573.

Canagaratna, M. R., Jayne, J. T., Jimenez, J. L., Allan, J. D., Alfarra, M. R., Zhang, Q., et al. (2007). Chemical and Microphysical Characterization of Ambient Aerosols with the Aerodyne Aerosol Mass Spectrometer. *Mass. Spectrom. Rev.*, 26:185–222

Canagaratna, M. R., Onasch, T. B., Wood, E. C., Herndon, S. C., Jayne, J. T., Cross, E. S., et al. (2010). Evolution of Vehicle Exhaust Particles in the Atmosphere. *J. Air & Waste Manag. Assoc.* 60:1192–1203, DOI: 10.3155/1047-3289.60.10.1192.

Cozic, J., Verheggen, B., Mertes, S., Connolly, P., Bower, K., Petzold, A., et al. (2007). Scavenging of Black Carbon in Mixed Phase Clouds at the High Alpine Site Jungfraujoch. *Atmos. Chem. Phys.*, 7:1797–1807, DOI: 10.5194/acp-7-1797-2007.

Cross, E. S., Onasch, T. B., Ahern, A. T., Wrobel, W., Slowik, J. G., Olfert, J., et al. (2010). Soot Particle Studies –Instrument Intercomparison–Project Overview. *Aerosol Sci. Tech.*, 44: 592–611.

DeCarlo, P. F., Kimmel, J. R., Trimborn, A., Northway, M. J., Jayne, J. T., Aiken, A. C., et al. (2006). Field-Deployable, High-Resolution, Time-of-Flight Aerosol Mass Spectrometer. *Anal. Chem.*, 78:8281–8289.

Demerjian, K. L., and Mohnen, V. A. (2008). Synopsis of the Temporal Variation of Particulate Matter Composition and Size. *J. Air Waste Manage.*, 58:216–233.

Di Filippo, P., Riccardi, C., Pomata, D., and Buiarelli, F. (2010). Concentrations of PAHs and Nitro-and Methyl-Derivatives Associated with A Size-Segregated Urban Aerosol. *Atmos. Environ.* 44:2742–2749.

Dockery D. W., Pope C. A., Xu X., Spengler, J. D., Wave, J. H., Fay, M. E., et al. (1993). An Association Between Air Pollution and Mortality in Six US Cities. *N. Engl. J. Med.* 329:1753–1759.

Dockery, D. W., and Stone, P. H. (2007). Cardiovascular Risks from Fine Particulate Air Pollution. *New Engl. J. Med.*, 356:511–513

Drewnick, F., Jayne, J. T., Canagaratna, M. R., Worsnop, D. R., and Demerjian, K. L. (2004b). Measurement of Ambient Aerosol Composition during the PMTACS-NY 2001 using an Aerosol Mass Spectrometer, Part II: Chemically Speciated Mass Distributions. *Aerosol Sci. Technol.* 38:104–117.

Drewnick, F., Schwab, J. J., Jayne, J. T., Canagaratna, M. R., Worsnop, D. R., and Demerjian, K. L. (2004a). Measurement of Ambient Aerosol Composition during the PMTACS-NY 2001 using an Aerosol Mass Spectrometer, Part I: Mass Concentrations. *Aerosol Sci. Technol.* 38:92–103.

Durant, J. L., Ash, C. A., Wood, E. C., Herndon, S. C., Jayne, J. T., Knighton, W. B., et al. (2010). Short-Term Variation in Near-Highway Air Pollutant Gradients on a Winter Morning. *Atmos. Chem. Phys.*, 10:5599–5626.

Dutkiewicz, V. A., Qureshi, S., Husain, L., Schwab, J. J., and Demerjian, K. L. (2006). Elemental Composition of PM2.5 Aerosols in Queens, New York: Evaluation of Sources of Fine-Particle Mass. *Atmos. Environ.*, 40:347–359.

Dutkiewicz, V. A., Qureshi, S., Khan, A. R., Ferraro, V., Schwab, J., Demerjian, K., and Husain, L. (2004). Sources of Fine Particulate Sulfate in New York. *Atmos. Environ.*, 38:3179–3189.

Environmental Protection Agency (EPA). (2002). Diesel Exhaust in the Unites States. Available at http://www.epa.gov/otaq/retrofit/documents/f020448.pdf

Environmental Protection Agency (EPA). (2008). Integrated Review Plan for National Ambient Air Quality Standards for Particulate Matter. Available at http://www.epa.gov/ttn/naaqs/standards/pm/data/2008_03_final_integrated_review_plan.pdf

Gao, R. S., Schwarz, J. P., Kelly, K. K., Fahey, D. W., Watts, L. A., Thompson, T. L., et al. (2007). A Novel Method for Estimating Light-Scattering Properties of Soot Aerosols Using a Modified Single-Particle Soot Photometer. *Aerosol Sci. Technol.*, 41:125–135.

Gehrig, R., Hill, M., Buchmann, B., Imhof, D., Weingartner, E., and Baltensperger, U. (2004). Separate Determination of PM10 Emission Factors of Road Traffic for Tailpipe Emissions and Emissions from Abrasion and Resuspension Processes. *Int. J.Env.Poll.*, 22:312–325.

Green, R. S., Malig, B., Windham, G. C., Fenster, L., Ostro, B., and Swan, S. (2009). Residential Exposure to Traffic and Spontaneous Abortion. *Environ. Health Perspect.*, 117(12): 1939–1944.

Hagler, G. S. W., Baldauf, R. W., Thoma E. D., Long, T. R., Snow, R. F., Kinsey, J. S., et al. (2009). Ultrafine Particles Near a Major Roadway in Raleigh, North Carolina: Downwind Attenuation and Correlation with Traffic-Related Pollutants. *Atmos. Environ.*, 43:1229–1234.

Harrison, R., Beddows, D. C. S., and Dall'Osto, M. (2011). PMF Analysis of Wide-Range Particle Size Spectra Collected on a Major Highway. *Environ. Sci. Technol.*, 45:5522–5528. dx.doi.org/10.1021/es2006622.

Herndon, S. C., Onasch, T. B., Frank, B. P., Marr, L. C., Jayne, J. T., Canagaratna, M. R., et al. (2005). Particulate Emissions from in-use Commercial Aircraft. *Aerosol Sci. Technol.*, 39(8):799–809, DOI: 10.1080/02786820500247363

Hu, S., Fruin, S., Kozawa, K., Mara, S., Paulson, S. E., and Winer, A. M. (2009). A Wide Area of Air Pollutant Impact Downwind of a Freeway During Pre-Sunrise Hours. *Atmos. Environ.*, 43:2541–2549.

Imhof, D., Weingartner, E., Prevot, A. S., Ordonez, C., Kurtenback, R., Wiesen, P., et al. (2006). Aerosol and NOx Emission Factors and Submicron Particle Number Size Distributions in Two Road Tunnels with Different Traffic Regimes. *Atmos. Chem. Phys.*, 6:2215–2230.

IPCC: Fourth Assessment Report. (2007). The Physical Science Basis, Working Group I, Final Report, Geneva, Switzerland. available at: http://www.ipcc.ch/ipccreports/ar4-wg1.htm.

Jacobson, M. Z. (2001). Strong Radiative Heating due to the Mixing State of Black Carbon in Atmospheric Aerosols. *Nature*, 409:695–697.

Jayaratne, E. R., He, C., Ristovski, Z. D., Morawska, L., and Johnson, C. R. (2008). A Comparative Investigation of Ultrafine Particles Number and Mass Emissions from a Fleet of On-Road Diesel and CNG Buses. *Environ. Sci. Technol.*, 42:6736–6742.

Jimenez, J. L., Canagaratna, M. R., Donahue, N. M., Prevot, A. S. H., Zhang, Q., Kroll, J. H., DeCarlo, P. F., et al. (2009). Evolution of Organic Aerosols in the Atmosphere. *Science*, 326:1525–1529, 2009. DOI: 10.1126/science.1180353.

Karner, A. A., Eisinger, D. I., and Niemeier, D. A. (2010). Near-Roadway Air Quality: Synthesizing the Findings from Real-World Data. *Environ. Sci. Technol.*, 44:5334–5344.

Kirchstetter, T. W., Harley, R. A., Kreisberg, N. M., Stolzenburg, M. R., and Hering, S. (1999). On-Road Measurement of Fine Particle and Nitrogen Oxide Emissions from Light and Heavy-Duty Motor Vehicles. *Atmos. Env.* 33:2955–2968.

Kittelson, D. (1998). Engines and Nanoparticles: A Review. *J. Aerosol Sci.*, 29:575–588.

Kittelson, D. B., Watts, W. F., Johnson, J. P., Thorne, C., Higham, C., Payne, M., et al. (2008). Effect of Fuel and Lube Oil Sulfur on the Performance of a Diesel Exhaust Gas Continuously Regenerating Trap. *Environ. Sci. Technol.*, 42:9276–9282.

Kleeman, M. J., Schauer, J. J., and Cass, G. E. (2000). Size and Composition Distribution of Fine Particulate Matter Emitted from Motor Vehicles. *Environ. Sci. Technol.*, 34:1132–1142.

Knol, A. B., de Hartog, J. J., Boogaard, H., Slottje, P., van der Sluijs, J. P., Lebret, E., et al. (2009). Expert Elicitation on Ultrafine Particles: Likelihood of Health Effects and Causal Pathways. *Particle Fibre Toxicol.*, 6(19):1, DOI: 10.1186/1743-8977-6-19. Available online at: http://www.particleandfibretoxicology.com/content/6/1/19/ref.

Kolb, C. E., Herndon, S. C., McManus, J. B., Shorter, J., Zahniser, M., Nelson, D., et al. (2004). Mobile Laboratory with Rapid Response Instruments for Real-Time Measurements of Urban and Regional Trace Gas and Particulate Distribution and Emission Source Characteristics. *Environ. Sci. Technol.*, 38:5694–5703.

Downloaded by [Institute Of Atmospheric Physics] at 20:09 13 July 2012

Downloaded by [Institute Of Atmospheric Physics] at 20:09 13 July 2012

Kupiainen K., and Pirjola L. (2011). Vehicle Non-exhaust Emissions from the Tire-Road Interface–Effect of Stud properties, Traction Sanding and Resuspension. *Atmos. Environ*, 45(N25): 4141–4146.

Lin, Y. C., Schwab, J. J., Demerjian, K. L., Bae, M.-S., Chen, W.-N., Sun, Y., et al. (2011). Summertime Formaldehyde Observations in New York City: Ambient levels, Sources and Its Contribution to HOx Radicals. *J. Geophys. Res.*, 117: D08305, DOI: 10.1029/2011JD016504

Liu, P. S.K., Deng, R., Smith, K. A., Williams, L. R., Jayne, J. T., Canagaratna, M. R., et al. (2007). Transmission Efficiency of an Aerodynamic Focusing Lens System: Comparison of Model Calculations and Laboratory Measurements for the Aerodyne Aerosol Mass Spectrometer. *Aerosol Sci. Technol.*, 41(8):721–733, DOI: 10.1080/02786820701422278

Lubick, N. (2009). Breathing Less Easily with Ultrafine Particles. *Environ. Sci. Technol.*, 43(N13): 4615–4617, DOI: 10.1021/es901328h.

Maricq, M. M., and Maldonado, H. (2009). Directions for Combustion Engine Aerosol Measurement in the 21st Century. *J. Air and Waste Manage. Assoc.*, 60:1165–1176, DOI: 10.3155/1047-3289.60.10.1165.

Massoli, P., Kebabian, P. L., Onasch, T. B., Hills, F. B., and Freedman, A. (2010). Aerosol Light Extinction Measurements by Cavity Attenuated Phase Shift (CAPS) Spectroscopy: Laboratory Validation and Field Deployment of a Compact Aerosol Particle Extinction Monitor. *Aerosol Sci. Technol.*, 44(6): 428–435, DOI: 10.1080/02786821003716599.

McAuley, T. (2010). Spatial Measurements of Ultrafine Particles Using an Engine Exhaust Particle Sizer TM within a Local Community Downwind of a Major International Trade Bridge in Buffalo, New York. *Aerosol Sci. Technol.*, 44:1096–1104, DOI: 10.1080/02786826.2010.512026

Morawska, L., Ristovski, Z., Jayaratne, E. R., Keogh, D. U., and Ling, X. (2008). Ambient Nano- and Ultrafine Particles from Motor Vehicle Emissions: Characteristics, Ambient Processing and Implications on Human Exposure. *Atmos. Environ.*, 42:8113–8138.

Ng, N. L., Canagaratna, M. R., Zhang, Q., Jimenez, J. L., Tian, J., Ulbrich, I. M., et al. (2010). Organic Aerosol Components Observed in Northern Hemispheric Datasets from Aerosol Mass Spectrometry. *Atmos. Chem. Phys.*, 10:4625–4641, DOI: 10.5194/acp-10-4625-2010.

Ng, N. L., Canagaratna, M. R., Jimenez, J. L., Zhang, Q., Ulbrich, I. M., and Worsnop, D. R. (2011b). Real-Time Methods for Estimating Organic Component Mass Concentrations from Aerosol Mass Spectrometer Data. *Environ. Sci. Technol.*, 45:910–916.

Ng, N. L., Herndon, S. C., Trimborn, A., Canagaratna, M. R., Croteau, P. L., Onasch, T. B., et al. (2011a). An Aerosol Chemical Speciation Monitor (ACSM) for Routine Monitoring of the Composition and Mass Concentrations of Ambient Aerosol. *Aerosol Sci. Technol.*, 45(7):780–794, DOI: 10.1080/02786826.2011.560211.

Ning, Z., Polidori, A., Schauer, J. J., and Sioutas, C. (2008). Emission Factors of PM Species Based on Freeway Measurements and Comparison with Tunnel and Dynamometer Studies, *Atmos. Environ.*, 42:3099–3114.

Onasch, T. B., Jayne, J. T., Herndon, S. C., Worsnop, D. R., Miake-Lye, R. C., Mortimer, I. P., et al. (2009). Chemical Properties of Aircraft Engine Particulate Exhaust Emissions. *J. Propul. Power*, 25:1121–1137.

Onasch, T.B, Trimborn, A., Fortner, E., Jayne, T. J., Kok, G. L., Williams, L., et al. (2012). Soot Particle Aerosol Mass Spectrometer: Development, Application and Initial Validation. *Aerosol Sci. Technol.*, 46:804–817, DOI: 10.1080/02786826.2012.663948.

Paatero, P., and Tapper, U. (1994). Positive Matrix Factorization: A Non-Negative Factor Model with Optimal Utilization of Error Estimates of Data Values. *Environmetrics*, 5:111–126.

Pedersen, C. B., O. Raaschou-Nielsen, O. Hertel, and Mortensen, P. B. (2004). New Directions: Air Pollution from Traffic and Schizophrenia Risks, *Atmos. Environ.*, 38(22):3733–3734.

Perez, L., Medina_Ramon, M., Kunzli, N., Alastuey, A., Pey, J., Perez, N., et al. (2009). Size Fractionate Particulate Matter, Vehicle Traffic, and Case-Specific Daily Mortality in Barcelona, Spain. *Environ. Sci. Technol.*, 43:4707–4714, DOI: 10.1021/es8031488.

Petzold, A., Kramer, H., and Schonlinner, M. (2002). Continuous Measurement of Atmospheric Black Carbon Using a Multi-Angle Absorption Photometer. *Environ. Sci. Poll. Res.* 4:78–82.

Petzold, A., and Schonlinner, M. (2004). Multiangle Absorption Photometry—A New Method for the Measurement of Aerosol Light Absorption and Atmospheric Black Carbon. *J. Aerosol Sci.*, 35:421–441.

Petzold, A., Schloesser, H., Sheridan, P. J., Arnott, W. P., Ogren, J. A., and Virkkula, A. (2005). Evaluation of Multi-angle Absorption Photometry for Measuring Aerosol Light Absorption. *Aerosol Sci. Technol.* 39:40–51.

Pirjola, L., Paasonen, P., Pfeiffer, D., Hussein, T., H¨ameri, K., Koskentalo, T., et al. (2006). Dispersion of Particles and Trace Gases Nearby a City Highway: Mobile Laboratory Measurements in Finland, *Atmos. Environ.*, 40:867–879.

Pope, C. A., Burnett, R. T., Thun, M. J., Calle, E. E., Krewski, D., Ito, K., et al. (2002). Lung Cancer, Cardiopulmonary Mortality, and Long–Term Exposure to Fine Particulate Air Pollution. *J. Am. Med. Assoc.*, 287:1132–1141.

Pope, C. A. III, and Dockery, D. W. (2006). Health Effects of Fine Particulate Air Pollution: Lines That Connect. *J. Air Waste Manage. Assoc.*, 56(6):709–742.

Pope, C. A., Ezzati, M., and Dockery, D. W. (2009). Fine-Particulate Air Pollution and Life Expectancy in the United States. *N. Engl. J. Med.*, 360:376–386, DOI: 10.1056/NEJMsa0805646.

Russell, A. G., and Brunekreef, B. (2009). A Focus on Particulate Matter and Health. *Environ. Sci. Technol.*, 43(N 13):4620–4625.

Schauer, J. J., Kleeman, M. J., Cass, G. R., and Simoneit, B. R.T. (1999). Measurements of Emissions from Air Pollution Sources. 2. C_1 Through C_{30} Organic Compounds from Medium Duty Diesel Trucks. *Environ. Sci. Technol.*, 33:1578–1587.

Schauer, J. J., Kleeman, M. J., Cass, G. R., and Simoneit, B. R.T. (2002). Measurements of Emissions from Air Pollution Sources. 5. C_1 Through C_{32} Organic Compounds from Gasoline-Powered Motor Vehicles. *Environ. Sci. Technol*., 36:1169–1180.

Schneider, J., Hock, B. N., Weimer, S., Borrmann, S., Kirchner, U., Vogt, R., et al. (2005). Nucleation Particles in Diesel Exhaust: Composition Inferred from In-Situ Mass Spectrometric Analysis. *Environ. Sci. Technol.*, 39:6153–6161.

Schwarz, J. P., Gao, R. S., Fahey, D. W., Thomson, D. S., Watts, L. A., Wilson, J. C., et al. (2006). Single-Particle Measurements of Midlatitude Black Carbon and Light Scattering Aerosols from the Boundary Layer to the Lower Stratosphere, *J. Geophys. Res.*, 111:D16207, DOI: 10.1029/2007JD007076.

Seigneur, C. (2009). Current Understanding of Ultrafine Particulate Matter Emitted from Mobile Sources. *J. Air & Waste Manage. Assoc.* 59:3–17, DOI: 10.3155/1047-3289.59.1.3.

Shah, S. D., Cocker, D. R., Miller, J. W., and Norbeck, J. M. (2004). Emission Rates of Particulate Matter and Elemental and Organic Carbon from In-Use Ddiesel Engines. *Environ. Sci. Technol.*, 38:2544–2550.

Shorter, J. H., Herndon, S., Zahniser, M. S., Nelson, D. D., Wormhoudt, J., Demerjian, K. L., et al. (2005). Real-Time Measurements of Nitrogen Oxide Emissions from In-Use New York City Transit Buses Using A Chase Vehicle. *Environ. Sci. Technol.*, 39:7991–8000.

Stanek, L. W., Sacks, J. D., Dutton, S. J., and Dubois, J. J.B. (2011). Attributing Health Effects to Apportioned Components and Sources of Particulate Matter: An Evaluation of Collective Results. *Atmos. Environ.* 45:5655–5663.

Strawa, A. W., Kirchstetter, T. W., Hallar, A. G., Ban-Weiss, G. A., McLaughlin, J. P., Harley, R. A., et al. (2010). Optical and Physical Properties of Primary On-Road Vehicle Particle Emissions and Their Implications for Climate Cchange. *J. Aer. Sci.*, 41:35–60, DOI: 10.1016/j.aerosci.2009.08.010.

Sueper, D. (2010). ToF-AMS Analysis Software. available at: http://cires.colorado.edu/jimenez-group/ToFAMSResources/ ToFSoftware/index.html.

Sun, Y. L., Zhang, Q., Schwab, J. J., Chen, W. N., Bae, M. S., Lin, Y. C., et al. (2011b). A Case Study of Aerosol Processing and Evolution in Summer in New York City. *Atmos. Chem. Phys.*, 11:12737–12750, DOI: 10.5194/acp-11-12737-2011.

Sun, Y. L., Zhang, Q., Schwab, J. J., Chen, W.-N., Bae, M.-S., Hung, H.-M., et al. (2012). Characterization of Near-Highway Submicron Aerosols in New York City with a High-Resolution Time-of-Flight Aerosol Mass Spectrometer. *Atmos. Chem. Phys.*, 12:2215–2227, DOI: 10.5194/acp-12-2215-2012.

Sun, Y. L., Zhang, Q., Schwab, J. J., Demerjian, K. L., Chen, N. W., Bae, S. M., et al. (2011a). Characterization of the Sources and Processes of Organic and Inorganic Aerosols in New York City with A High-Resolution Time-of-Flight Aerosol Mass Spectrometer. *Atmos. Chem. Phys.*, 11:1581–1602, DOI: 10.5194/acp-11-1581-2011.

Ulbrich, I. M., Canagaratna, M. R., Zhang, Q., Worsnop, D. R., and Jimenez, J. L. (2009). Interpretation of Organic Components from Positive Matrix Factorization of Aerosol Mass Spectrometric Data. *Atmos. Chem. Phys.*, 9:2891–2918.

Watson, J. G. (2002). Visibility: Science and Regulation. *J. Air Waste Manage.*, 52:628–713.

Weimer, S., Drewnick, F., Hogrefe, O., Schwab, J. J., Rhoads, K., Orsini, D., et al. (2006). Size-Selective Non-Refractory Ambient Aerosol Measurements During the Particulate Matter Technology Assessment and Characterization Study–New York 2004 Winter Intensive in New York City. *J. Geophys. Res.*, 111:D18305, DOI: 10.1029/2006JD007215.

WHO (2002). *World Health Report*. World Health Organization, Geneva.

Wood, E. C., Wormhoudt, J., Herndon, S. C., Jayne, J. T., Onasch, T. B., Knighton, B. W., et al. Is Nitrogen Dioxide a Good Indicator of Pollution?, in preparation.

Zhang, K. M., and Wexler, A. S. (2004). Evolution of Particle Number Distribution Near Roadways. Part I: Analysis of Aaerosol Dynamics Ad Its Implications for Engine Emission Measurements. *Atmos. Environ.* 38(38):6643–6653.

Zhang, K. M., Wexler, A. S., Niemeier, D. A., Zhu, Y. F., Hinds, W. C., and Sioutas, C. (2005a). Evolution of Particle Number Distribution Near Roadways. Part III: Traffic Analysis and On-Road Size Resolved Particulate Emission Factors. *Atmos. Environ.* 39(22):4155–4166.

Zhang, K. M., Wexler, A. S., Zhu, Y. F., Hinds, W. C., and Sioutas, C. (2004). Evolution of Particle Number Distribution Near Roadways. Part II: The "Road-to-Ambient" Process. *Atmos. Environ.* 38(38):6655–6665.

Zhang, Q., Alfarra, M. R., Worsnop, D. R., Allan, J. D., Coe, H., Canagaratna, M. R., et al. (2005b). Deconvolution and Quantification of Hydrocarbon-Like and Oxygenated Organic Aerosols Based on Aerosol Mass Sspectrometry. *Environ. Sci. Technol.*, 39:4938–4952, DOI: 4910.1021/es048568l

Zhang, Q., Canagaratna, M. C., Jayne, J. T., Worsnop, D. R., and Jimenez, J. L. (2005c). Time and Size-Resolved Chemical Composition of Submicron Particles in Pittsburgh - Implications for Aerosol Sources and Processes. *J. Geophys. Res.*, 110:D07S09, DOI: 10.1029/2004JD004649

Zhang, Q., Jimenez, J. L., Canagaratna., M. R., Ulbrich, I. M., Ng, N. L., Worsnop, D. R., et al. (2011). Understanding Atmospheric Organic Aerosols via Factor Analysis of Aerosol Mass Spectrometry: A Review. *Anal. Bioanal. Chem*, 401:3045–3067, DOI: 10.1007/s00216-011-5355y.

Zhang, Q., Worsnop, D. R., Canagaratna, M. R., and Jimenez, J. L. (2005d). Hydrocarbon-Like and Oxygenated Organic Aerosols in Pittsburgh: Insights into Sources and Processes of Organic Aerosols. *Atmos. Chem. Phys.*, 5:3289–3311, DOI: 10.5194/acp-5-3289

Zhu, Y., Hinds, W. C., Kim, S., and Sioutas, C. (2002a). Concentration and Size Distribution of Ultrafine Particles Near a Major Highway. *J. Air Waste Manage. Assoc.*, 52:1032–1042.

Zhu, Y., Hinds, W. C., Kim, S., Shen, S., and Sioutas, C. (2002b). Study of Ultrafine Particles near a Major Highway with Heavy-Duty Diesel Traffic. *Atmos. Environ.*, 36:4323–4335.

Zhu, Y., Hinds, W. C., Shen, S., and Sioutas, C. (2004). Seasonal Trends of Concentration and Size Distribution of Ultrafine Particles Near Major Highways in Los Angeles. *Aerosol Sci. Technol.*, 38(S1):5–13

Zhu, Y., Kuhn, T., Mayo, P., and Hinds, W. C. (2006). Comparison of Daytime and Nighttime Concentration Profiles and Size Distributions of Ultrafine Particles Near a Major Highway. *Environ. Sci. Technol.*, 40:2531–2536.

Zou, B., Wilson, G., Zhan, F. J., and Zen, Y. (2009). Spatially Differentiated and Source-Specific Population Exposure to Ambient Urban Air Pollution. *Atmos. Environ.*, 43:3981–3988, DOI: 10.1016/j.atmosenv.2009.05.022.

Downloaded by [Institute Of Atmospheric Physics] at 20:09 13 July 2012